Superradiant Cooling, Trapping and Lasing of Dipole-Interacting Clock Atoms

Masterarbeit

zur Erlangung des akademischen Grades
Master of Science
(MSc)

eingereicht an der
Fakultät für Mathematik, Informatik und Physik
der Universität Innsbruck

von
Christoph Hotter, BSc

Betreuer:
Univ. Prof. Dr. Helmut Ritsch

Institut für Theoretische Physik

Innsbruck, Dezember 2018

Abstract

We study a generic laser model based on a cold ensemble of clock atoms in an optical resonator. The atoms are modelled as two-level point particles incoherently pumped from the side. Collective effects arising from dipole-dipole interaction of the closely spaced atoms are included and motion of the particles along the cavity axis is described in a semi-classical treatment. The light field inside the resonator is described by a single frequency mode and the atoms couple to it via the common Tavis-Cummings interaction. The intracavity photons leak through the cavity mirrors with some loss rate, which is much higher than the spontaneous emission rate of a clock atom.

Due to technical noise issues it seems to be very challenging to go below the striking spectral linewidth limit of approximately the Hz-level reached nowadays by ordinarily operating laser systems. Hence a concept, already invented more than two decades ago, is receiving more attention in the last few years, the so-called superradiant laser. A laser that has been predicted to go beyond the mHz-level with an extreme frequency stability.

To analyze different properties of such a superradiant laser we use numerical methods to directly simulate systems of a few atoms arranged along the cavity axis. By scanning the experimentally most tunable system parameters we find regimes in which lasing, cooling and trapping is possible by only pumping the atoms incoherently. For sufficiently slow initial particles the light field scattered by the atoms into the cavity is strong enough to keep them at the intensity maxima. The cooling mechanism leads to an increasingly precise localization of the atoms until a certain final temperature is reached. This features almost equivalent coupling of the atoms to the cavity field, which is needed for the superradiant lasing process.

Investigating the laser properties shows that they do not exhibit a significant difference to a model with fixed particle positions. The spectrum is less sensitive on cavity fluctuations compared to a conventional operating laser and we observe average photon numbers inside the cavity below one, as expected for a superradiant laser.

Zusammenfassung

Wir untersuchen ein allgemeines Lasermodell basierend auf einem Ensemble von kalten Uhren-Atomen in einem optischen Resonator. Die Atome sind als Zwei-Level Punktteilchen modelliert, die inkohärent von der Seite gepumpt werden. Kollektive Effekte, hervorgerufen durch Dipol-Dipol Wechselwirkung von dicht nebeneinander befindlichen Atomen werden berücksichtigt und die Bewegung der Teilchen wird durch semiklassische Gleichungen beschrieben. Das Lichtfeld im Resonator wird durch eine einzelene Frequenzmode beschrieben und die Atome koppeln zu dieser über die übliche Tavis-Cummings Wechselwirkung. Die Photonen im Resonator verlassen diesen durch die Spiegel mit einer bestimmten Verlustrate, welche viel höher ist als die spontane Emissionsrate eines Uhren-Atoms.

Aufgrund von Problemen durch technisches Rauschen scheint es nur sehr schwer möglich zu sein das bisherige Limit der spektralen Linienbreite von etwa einem Hertz zu unterschreiten, welches derzeit von gewöhnlich funktionierenden Lasersystem erreicht werden kann. Dadurch bekam ein Konzept, das schon vor mehr als zwei Jahrzehnten entwickelt wurde, in den letzen Jahren mehr Aufmerksamkeit, der superradiante Laser. Ein Laser dem vorhergesagt wird Linienbreiten bis unter das mHz-Level zu erreichen mit extremer Frequenzstabilität.

Um verschiedene Eigenschaften eines solchen superradianten Lasers zu analysieren verwenden wir numerische Methoden. Wir simulieren Systeme von wenigen Atomen, die sich entlang der Spiegelachse bewegen. Durch scannen von den experimentell am einfachsten zugänglichen Parametern haben wir Bereiche gefunden bei denen ein Laserbetrieb mit gleichzeitigem Kühlen und Fangen der Atome möglich ist, wobei dafür lediglich die Atome inkoherent gepumpt werden müssen. Für Teilchen die anfänglich langsam genug sind reicht das entstandene Lichtfeld im Resonator aus um sie an den Intensitätsmaxima zu lokalisieren. Das Kühlen führt zu einer immer besseren Lokalisierung der Atome an den Intensitätsmaxima bis eine bestimmte Endtemperatur erreicht wird. Dies ermöglicht nahezu gleiches Koppeln aller Atome an das Lichtfeld, welches für den superradianten Laserprozess benötigt wird.

Das Untersuchen der Lasereigenschaften zeigt, dass diese keine signifikanten Unterschiede zu einem Model mit fixen Teilchenpositionen aufweisen. Das Spektrum ist weniger von Resonatorfluktuationen abhängig als das eines herkömmlich funktionierenden Lasers und wir beobachten eine durchschnittliche Photonenanzahl unter Eins im Resonator, wie erwartet von einem superradianten Laser.

Danksagung

Zuerst möchte ich meiner Familie danken, speziell aber meinen Eltern die mich immer moralisch sowie finanziell unterstützt haben und somit mir dieses Studium erst möglich gemacht haben.

Ein großer Dank gilt auch der kompletten Arbeitsgruppe auszusprechen, die mich nicht nur alle sehr freundlich aufgenommen haben, sondern auch stets eine große Hilfe bei all meinen Fragen und Problemen waren. Besonderer Dank gilt hierbei David Plankensteiner und Laurin Ostermann die mir immer beide mit sehr viel Motivation und Engagement halfen meine Probleme zu lösen. Natürlich wäre all dies nicht ohne meinen Betreuer Prof. Helmut Ritsch möglich gewesen, bei dem ich mich nicht nur für die Möglichkeit bedanke an einem so interessanten Thema arbeiten zu dürfen, sondern auch für seine stets sehr hilfreichen Diskussionen und Antworten auf meine Fragen.

Selbstverständlich bedanke ich mich auch bei meinen Freunden die mich immer unterstützt haben sowie auch allen Studienkollegen, ohne die die komplette Studienzeit niemals so nett gewesen wäre.

Abschließend bedanke ich mich noch bei allen nicht Genannten, die hoffentlich nicht zu viele sind.

Contents

Chapter 1.

Introduction

The applications of lasers in science, industry and also the daily life are numerous. Depending on their utilization they need to have different capabilities. Lasers are able to emit coherent light with a stable intensity and a very small bandwidth. In this thesis we focus on a laser operating in the regime of an extreme frequency stability but also accuracy, far below the current technical limit of conventional laser systems. A fundamental example for the usage of such a frequency-stable laser is the operation of an atomic clock, which leads to a more precise time measurement and thus a manifold of applications, such as testing of fundamental laws of Physics or much more accurate GPS-navigation.

A common laser operates in the good cavity regime $\Gamma \gg \kappa$, with Γ the spontaneous emission rate of the excited atom and κ the photon loss rate through the cavity mirrors.

The theoretical spectral linewidth limit $\Delta\nu_{\mathrm{ST}}$ is given by the Schawlow-Townes linewidth [1]. In the good cavity regime we find $\Delta\nu_{\mathrm{ST}} \sim \kappa/n$, with n the average intracavity photon number. For such a laser it is possible to reduce the linewidth by increasing the number of photons in the cavity. A striking spectral linewidth below 1Hz has been reached in this regime, but further improvements seem to be very difficult. The main limitation for the further reduction of the linewidth of a conventional operating laser is thermal noise in the cavity mirrors, which leads to fluctuations in the cavity length and therefore also the frequency. To circumvent this problem it has been suggested theoretically, approximately ten years ago, to use an ultranarrow optical clock transition emitting into a high quality cavity [2], expected to exhibit a linewidth in the mHz range. Such a laser operates in the bad cavity regime $\Gamma \ll \kappa$, and is called superradiant laser. The name bad cavity regime can be somewhat misleading in this context, since the mirrors used in experiments are actually the best available at the moment. Due to the big difference between Γ and κ, the energy is dominantly stored in the atoms instead of the photons. This means there are only a few photons inside the cavity, therefore thermal cavity noise does not affect the light field much [3]. Extracting the emitted light from the clock transition directly would be the best way to get rid of the thermal noise, but unfortunately this spontaneously emitted light does not have enough power for practical applications. Also, the dipole moment of the two-level transition is very small, therefore only strong collective coupling of the atoms with the cavity mode can lead

to sufficiently high output power. Here superradiant emission from the atoms into the cavity field mode is responsible for the needed gain. The Schawlow-Townes linewidth in the bad cavity regime is proportional to $\Delta\nu_{\mathrm{ST}} \sim \Gamma^2/(\kappa n)$. As we want the intracavity photon number to be small to minimize the influence of the cavity fluctuations on the spectrum, we need to ensure that the $\Gamma/\kappa < n$ to achieve a narrow and stable linewidth. Some features of the superradiant laser, like intracavity photon numbers below one and a better insensibility on cavity length fluctuation, have already been shown experimentally to some extent [1].

The theory of a superradiant laser has already been described in 1993 [4], predicting a laser with an intensity proportional to the square and a linewidth to the inverse square of the atom number. The underlying mechanism is superradiant emission into the cavity mode. Dicke introduced the phenomenon of superradiance as coherent radiation arising from collective spontaneous emission of a gas of closely spaced two-level emitters, even proposing a mirrorless laser [5]. A detailed essay on this topic was penned by Haroche and Gross three decades later [6]. N two-level atoms confined in a volume small compared to a cube with side length equal to the transition wavelength, act like a rigid dipole, exhibiting collective spontaneous emission. While independent radiating atoms exhibit a spontaneous emission intensity proportional to N, the collective process emits a pulse which possesses an intensity maximum proportional to N^2. Repumping the atoms during emission in the laser setup leads to stationary instead of pulsed radiation. As mentioned above, the superradiant laser is predicted to exhibit a narrow linewidth proportional to $1/N^2$, in comparison the linewidth of collective spontaneous emission in free space is proportional to N. While the derivation of Dicke superradiance assumes the atoms to be confined in a small volume, for the superradiant laser this is not necessarily required, if one can ensure almost equal coupling of the atoms to the cavity field.

Including atomic motion in contrast to fixed particle positions [7] leads to varying atom-field coupling reducing the superradiance. A possible mechanism to resolve this problem is cooling and self-trapping of the atoms at the intensity maxima of the cavity mode [8]. For properly chosen parameters the result can be a cavity cooling process accompanied by lasing [9].

This thesis is structured as follows. In chapter 2 we show the theoretical concepts needed to describe the system, including atom-light interaction inside a cavity, collective behaviour, dissipative processes, semi-classical treatment, cavity cooling and laser theory. Chapter 3 combines all the concepts attained in the previous chapter and concludes in a set of semi-classical coupled differential equations defining our model. Results on the cooling and trapping process as well as the method used to obtain them are shown in chapter 4, where we also compare our results with that for independent atoms. Important lasing properties like the spectrum, second order correlation function, photon number and excited state population of the system are analyzed in chapter 5 by scanning over a set of stable parameters.

Chapter 2.

Basic Concepts

In this chapter we provide the theoretical concepts and mathematical tools needed to describe our laser model and calculate its dynamics.

2.1. Atom-Light Interaction Inside a Cavity

We describe the interaction of N particles with the light field inside an optical cavity [10]. It is well known that in a cavity with length l_c only modes with frequencies ω_c are allowed, where the corresponding wavelength $\lambda_\mathrm{c} = \omega_\mathrm{c} c/(2\pi)$ satisfies the property $l_\mathrm{c} = n\lambda_\mathrm{c}/2$, with $n \in \mathbb{N}$ and c the speed of light. As commonly done in cavity quantum electrodynamics we treat our atoms as two-level atoms and neglect all light modes inside the cavity except the one resonant. These two approximations are valid if the internal structure of the atom is such that the transition frequency of two levels of the atom is close to resonance with the frequency of one mode of the cavity light field, and all other energy levels of the atom which could be occupied with some probability are off-resonant with all other cavity mode frequencies. We then call the lower energy state of the two-level atom ground state $|g\rangle$ and the higher energy state excited state $|e\rangle$. The transition frequency between these two states is ω_a, implying an energy gap of $\hbar\omega_\mathrm{a}$, with $\hbar$ the reduced Planck constant. We denote the frequency of the mode close to resonance to the atom transition by ω_c, then every photon inside the cavity possesses an energy of $\hbar\omega_\mathrm{c}$. The difference between ω_c and ω_a is called the detuning $\Delta = \omega_\mathrm{c} - \omega_\mathrm{a}$.

Now we will express the interaction between the atoms and the light field inside the cavity mathematically. Since we do not consider dissipative processes in this section, we only need to define the Hamiltonian operator for the system to describe it. This operator consists of three parts, as shown below. We are not providing a rigorous derivation of the Hamiltonian, but rather we shall illustrate the basic concepts.

The energy of a single-mode light field inside a cavity can be described very elegantly with the bosonic ladder operators $a^\dagger$ and a. The action of $a^\dagger$ and a correspond to creating and annihilating a photon with frequency ω_c, respectively. We call $|n\rangle$ the state of a cavity with n photons inside, then the operators have the following properties

$$a^\dagger |n\rangle = \sqrt{n+1}\,|n+1\rangle \tag{2.1}$$
$$a\,|n\rangle = \sqrt{n}\,|n-1\rangle\,. \tag{2.2}$$

One can see that the operator product $a^\dagger a$ counts the number of photons inside the cavity, hence the Hamilton operator of the light field inside the cavity is

$$H_\mathrm{c} = \hbar\omega_\mathrm{c} a^\dagger a, \tag{2.3}$$

with $H_\mathrm{c}\,|n\rangle = \hbar\omega_\mathrm{c} n\,|n\rangle$. In a mathematically rigorous derivation we would end up with an additional term $\hbar\omega_\mathrm{c}/2$, often referred to as vacuum energy, but we can neglect this by simply employing an energy shift.

The energy of a two-level atom can be written in a similar way. Mathematically, the description of a two-level atom is the same as for a spin-1/2 particle. Hence we are allowed to treat our atoms as spin-1/2 particles and use the Pauli-Matrices to describe the internal dynamics. We choose the convention that $|g\rangle$ and $|e\rangle$ are eigenstates of σ_z, this means

$$\sigma_z\,|g\rangle = -\,|g\rangle \tag{2.4}$$
$$\sigma_z\,|e\rangle = +\,|e\rangle\,. \tag{2.5}$$

Therefore the Hamilton operator of the two-level atom is

$$H_\mathrm{a} = \frac{\hbar\omega_\mathrm{a}}{2}\sigma_z, \tag{2.6}$$

with the energy eigenvalues $-\hbar\omega_\mathrm{a}/2$ and $\hbar\omega_\mathrm{a}/2$. We introduce the fermionic operators σ^+ and σ^-. The action of them corresponds to exciting and deexciting the atom, respectively. This means the operators have the following properties

$$\sigma^+\,|g\rangle = |e\rangle \qquad \sigma^+\,|e\rangle = 0 \tag{2.7}$$
$$\sigma^-\,|e\rangle = |g\rangle \qquad \sigma^-\,|g\rangle = 0. \tag{2.8}$$

For reasons of convention we want the energy of the ground state to be zero, therefore we shift the energy of the Hamiltonian 2.6 using σ^+ and σ^- and obtain

$$H_\mathrm{a} = \hbar\omega_\mathrm{a}\sigma^+\sigma^-. \tag{2.9}$$

Using the formalism of bosonic and fermionic operators we can describe the interaction between an atom and the light field inside a cavity in a very intuitive way. We assume that an atom is placed at some position r along the cavity axis where the light field couples to it with some position-dependent strength $g(r)$, which we call coupling strength.

We implicitly assume here the radius of the atom to be much smaller than the wavelength of the intracavtiy light field, such that the entire atom feels the same light intensity. The interaction between the light field and the atom can be described by two possible processes, either the atom in the ground state absorbs a photon from the light field and becomes excited which corresponds to the operator $a\sigma^+$, or the atom in the excited state emits a photon into the cavity and deexcites which corresponds to the operator $a^\dagger\sigma^-$. Since these two processes are equal probable, the resulting interaction Hamiltonian is

$$H_{\text{int}} = \hbar g(r)[a\sigma^+ + a^\dagger\sigma^-]. \tag{2.10}$$

If we would rigorously derive the interaction Hamiltonian in the dipole approximation, we would additionally get terms proportional to $a\sigma^-$ and $a^\dagger\sigma^+$, but they can be neglected within the rotating wave approximation. The one-dimensional position-dependent expression for the coupling strength along the cavity axis is

$$g(r) = g\cos(k_{\text{c}}r), \tag{2.11}$$

with $k_{\text{c}} = \lambda_{\text{c}}/(2\pi)$ the wave vector of the cavity mode and g the coupling constant.

Putting the above parts together we get the full Hamiltonian operator of the atom-field system, for one atom at a fixed position, it is called the Jaynes-Cummings Hamiltonian [10]

$$H_{\text{JC}} = \hbar\omega_{\text{c}}a^\dagger a + \hbar\omega_{\text{a}}\sigma^+\sigma^- + \hbar g(r)[a\sigma^+ + a^\dagger\sigma^-]. \tag{2.12}$$

We can easily extend this system to N non-interacting atoms. The expression for $N > 1$ is called the Tavis-Cummings Hamiltonian [10]

$$H_{\text{TC}} = \hbar\omega_{\text{c}}a^\dagger a + \hbar\omega_{\text{a}}\sum_{i=1}^{N}\sigma_i^+\sigma_i^- + \hbar\sum_{i=1}^{N}g(r_i)[a\sigma_i^+ + a^\dagger\sigma_i^-]. \tag{2.13}$$

2.1.1. Rotating Frame

Changing to a rotating frame in a smart way can be a very useful tool to simplify the Hamiltonian of a system for numerical calculations. In this subsection we show a general procedure to switch to an arbitrary rotating frame and apply the method on our Hamiltonian 2.13.

We consider a time-dependent Hamiltonian $H(t)$, the state $|\Psi(t)\rangle$ fulfils the time dependent Schrödinger equation

$$i\hbar\partial_t|\Psi(t)\rangle = H(t)|\Psi(t)\rangle. \tag{2.14}$$

Now we define some unitary operator $R(t)$, we call it the rotation operator. We utilize this rotation operator to define a new state

$$|\Phi(t)\rangle = R(t)|\Psi(t)\rangle. \tag{2.15}$$

Since $R(t)$ is assumed unitary, we can calculate $|\Psi(t)\rangle$ from $|\Phi(t)\rangle$ using $|\Psi(t)\rangle = R^\dagger(t)\,|\Phi(t)\rangle$, therefore we only need to calculate the time evolution for $|\Phi(t)\rangle$ to obtain then $|\Psi(t)\rangle$. The time evolution of $|\Phi(t)\rangle$ is given by

$$\begin{aligned} i\hbar\partial_t\,|\Phi(t)\rangle &= i\hbar(\partial_t R(t))\,|\Psi(t)\rangle + i\hbar R(t)\partial_t\,|\Psi(t)\rangle \\ &= i\hbar\dot{R}(t)\,|\Psi(t)\rangle + R(t)H(t)\,|\Psi(t)\rangle \\ &= i\hbar\dot{R}(t)R^\dagger(t)\,|\Phi(t)\rangle + R(t)H(t)R^\dagger(t)\,|\Phi(t)\rangle\,. \end{aligned} \tag{2.16}$$

As you can see, $|\Phi(t)\rangle$ follows the time-dependent Schrödinger equation with a modified Hamiltonian

$$H' = i\hbar\dot{R}(t)R^\dagger(t) + R(t)H(t)R^\dagger(t). \tag{2.17}$$

Now we apply the above described method to our Hamiltonian. There are two possibilities which make sense, either to change into the rotating frame of the atoms, or into the rotating frame of the cavity. In our case it is not important in which frame we transform. We choose for the rotating frame of the atoms. In this case the rotating operator is

$$R(t) = e^{i\omega_\mathrm{a} t(a^\dagger a + \sum_{i=1}^N \sigma_i^+\sigma_i^-)}, \tag{2.18}$$

for the rotating frame of the cavity we only have to replace ω_a by ω_c. Now we calculate the modified Hamiltonian according to equation 2.17. One can easily check that the first term on the right-hand side in 2.17 is

$$i\hbar\dot{R}(t)R^\dagger(t) = -\hbar\omega_\mathrm{a}(a^\dagger a + \sum_{i=1}^N \sigma_i^+\sigma_i^-).$$

From the Hamiltonian 2.13 we get three contributions in the term $R(t)H(t)R^\dagger(t)$. Since operators acting on different Hilbertspaces always commute and an operator always commutes with itself, $\hbar\omega_\mathrm{c}a^\dagger a$ and $\hbar\omega_\mathrm{a}\sum_{i=1}^N \sigma_i^+\sigma_i^-$ do not change. In the last step we need to calculate $R(t)\hbar\sum_{i=1}^N g(r_i)[a\sigma_i^+ + a^\dagger\sigma_i^-]R^\dagger(t)$. By using the bosonic and fermionic commutation relations $[a^\dagger a, a] = -a$ and $[\sigma_i^+\sigma_i^-, \sigma_j^-] = -\delta_{ij}\sigma_i^-$, respectively, we see that the exponent of $R(t)$ commutes with $g(r_i)[a\sigma_i^+ + a^\dagger\sigma_i^-]$, hence also $R(t)$ commutes with it and we show that the interaction part also does not change.

Putting all parts from above together, we obtain the expression for the Tavis-Cummings Hamiltonian in the rotating frame of the atoms

$$H'_\mathrm{TC} = \hbar\Delta a^\dagger a + \hbar\sum_{i=1}^N g(r_i)[a\sigma_i^+ + a^\dagger\sigma_i^-]. \tag{2.19}$$

2.2. Open system dynamics - Master Equation

In the last section we only focused on closed systems satisfying energy conservation. It is well known, that the unitary time evolution of the density matrix ρ of such a lossless quantum system can be calculated with the von Neumann equation

$$\dot{\rho} = \frac{i}{\hbar}[\rho, H]. \tag{2.20}$$

In reality it is almost always the case that one has to deal with open systems. This means we have to include processes where energy leaks out or into the system. Taking the trace over the reservoirs coupled to the system leads to a very powerful and proven tool to describe dissipative processes in quantum optics, the Master equation [10, 11]

$$\dot{\rho} = \frac{i}{\hbar}[\rho, H] + \mathcal{L}[\rho]. \tag{2.21}$$

It features the same term as the von Neumann equation for the system plus an additional term, the Liouvillian superoperator $\mathcal{L}[\rho]$, which accounts for the dissipative processes. In this thesis, we do not derive the master equation or the Liovillian, but rather specify the different parts of it and describe them qualitatively. A rigorous derivation of the Master equation can be found in [12]. The master equation is said to be in Lindblad form, if the Liouvillian has the structure

$$\mathcal{L}[\rho] = \frac{1}{2}\sum_{i,j}\gamma_{ij}(2J_i\rho J_j^\dagger - J_i^\dagger J_j\rho - \rho J_i^\dagger J_j). \tag{2.22}$$

We call γ_{ij} rates and J_i are the jump operators which describe the dissipative process. The matrix generated by the coefficients γ_{ij} needs to be positive semidefinite to preserve the trace of the of the density matrix. In this form the last two terms are responsible for the dissipative process, while the first term preserves the trace, it is therefore called "recycling term". In the following we will only deal with Liouvillians in Lindblad form, this implies that we merely focus on Markovian processes [11], this means there is no back-action of the environment to the system.

In our model we include three different dissipative processes: cavity losses, incoherent pump of the two-level atom and collective spontaneous emission. The total Liouvillian is the sum of all of them [7]

$$\mathcal{L}[\rho] = \mathcal{L}_{\text{cav}}[\rho] + \mathcal{L}_{\text{pump}}[\rho] + \mathcal{L}_{\text{cd}}[\rho]. \tag{2.23}$$

2.2.1. Cavity Losses

The cavity losses describe the leaking of photons through the mirrors. The process is characterized by the loss rate κ, which denotes the rate of photons leaking out of the system on average. The smaller the value of κ the better are the mirrors. As one might

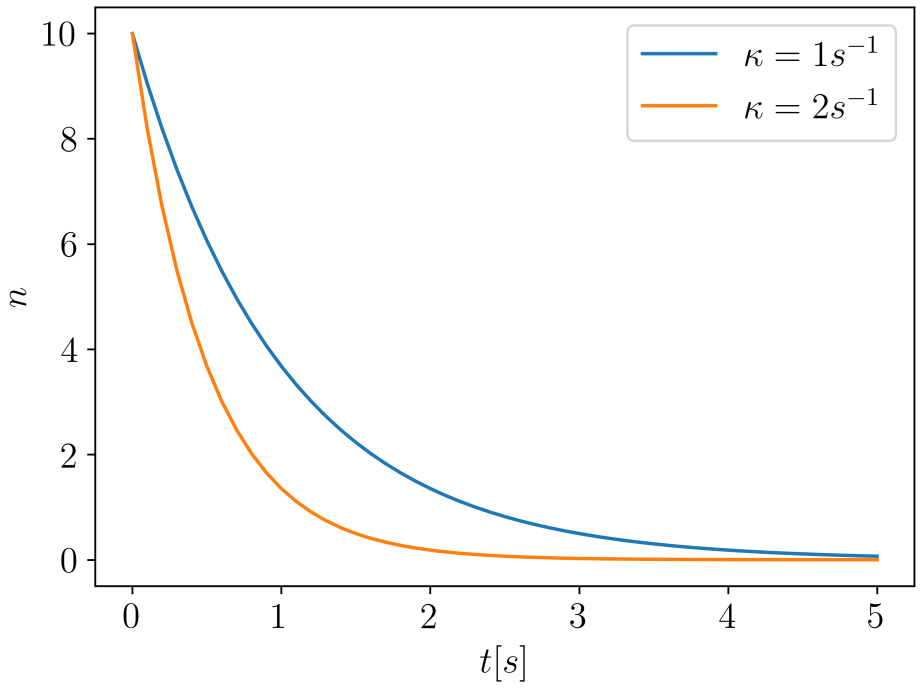

Figure 2.1.: *Exponential decay of photons through the cavity decay channel.* Higher values of the cavity loss rate κ correspond to faster photon decay. After the time $1/\kappa$ the amplitude A of the photon number reduces to A/e. We chose arbitrary values for κ.

intuitively guess, these jumps are described with the photon annihilation operator a. The expression for the Liouvillian is therefore [12]

$$\mathcal{L}_{\text{cav}}[\rho] = \frac{1}{2}\kappa(2a\rho a^\dagger - a^\dagger a\rho - \rho a^\dagger a). \tag{2.24}$$

This superoperator causes an exponential decay of the photon number inside the cavity. We demonstrate this in figure 2.1, by showing the time evolution of the photon number in a lossy cavity with initially 10 photons inside. There are no atoms in the cavity.

2.2.2. Collective Spontaneous Emission

The spontaneous emission of a photon from an excited atom with the inherent deexcitation of the atom is a well-known quantum jump phenomenon. Following the derivation of Wigner and Weißkopf [13] in the dipole approximation we obtain

$$\Gamma = \frac{\omega_{\text{a}}^3 \mu^2}{3\pi\epsilon_0 c^3} \tag{2.25}$$

for the spontaneous emission rate, which denotes the frequency of spontaneous emission events on average. The dipole moment of the atomic transition is denoted by $\vec{\mu}$, ϵ_0 is the dielectric constant and c the speed of light. The Liouvillian for the spontaneous emission of a photon from a single two-level atom is given by

$$\mathcal{L}_{\mathrm{sp}}[\rho] = \frac{1}{2}\Gamma(2\sigma^-\rho\sigma^+ - \sigma^+\sigma^-\rho - \rho\sigma^+\sigma^-), \tag{2.26}$$

described by the deexcitation operator σ^-. The basic idea of the derivation by Wigner and Weißkopf is to calculate the transition to the ground state in perturbation theory by interaction of a single atom with the quantized free (electro-magnetic) vacuum field. In section 2.3 we will show the result for an ensemble of N closely spaced emitters. The resulting collective rates form an $N \times N$ matrix which depends on the positions and dipole moments of the two-level atoms. The matrix elements are denoted by Γ_{ij}, specifying the influence of atom j on atom i. The decay of the i-th atom is described by the i-th atom deexcitation operators σ_i^-. Hence we get the expression for the Liouvillian of the collective spontaneous emission [14]

$$\mathcal{L}_{\mathrm{cd}}[\rho] = \frac{1}{2}\sum_{ij}\Gamma_{ij}(2\sigma_i^-\rho\sigma_j^+ - \sigma_i^+\sigma_j^-\rho - \rho\sigma_i^+\sigma_j^-). \tag{2.27}$$

2.2.3. Incoherent Pump

Population inversion of the two-level atom means that the excited state is occupied more than the ground state. This is not possible in thermal equilibrium. In order to obtain this we need to pump the atoms incoherently. In practise this can be done e.g. by coherently exciting an auxiliary state $|a\rangle$ which decays rapidly to the state $|e\rangle$, see figure 2.2. If the decay from the auxiliary state to the excited state is much faster than the decay from the excited to the ground state, we can neglect the population of the auxiliary state and describe the incoherent pump simply as an inverse spontaneous emission. This process is characterized by the pump rate R and as you might expect it is described by the excitation operator of the atom σ^+. If one would consider a level scheme where the decay from $|a\rangle$ to $|e\rangle$ is radiative, e.g. in a four-level model, we could also get collective effects here [4]. The Liouvillian in this case would look similar to the one in section 2.2.2, but with the operator σ_i^+ instead of σ_i^-. Since we do not focus on this, we treat our incoherent pump as independent.

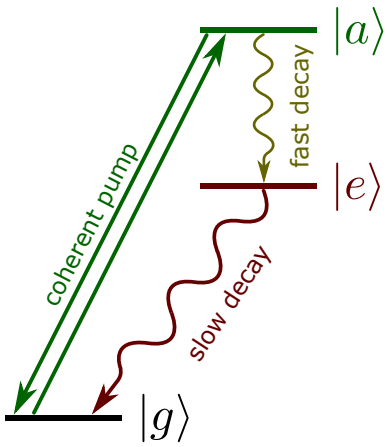

Figure 2.2.: *Schematics of an incoherent pump.* The decay from $|a\rangle$ to $|e\rangle$ needs to be much faster then the decay from $|e\rangle$ to $|g\rangle$.

The resulting Liouvillian for this is [2]

$$\mathcal{L}_{\text{pump}}[\rho] = \frac{1}{2}R\sum_i (2\sigma_i^+\rho\sigma_i^- - \sigma_i^-\sigma_i^+\rho - \rho\sigma_i^-\sigma_i^+). \tag{2.28}$$

2.3. Collective Dynamics

In our model we have to deal with an ensemble of closely spaced atoms, therefore we need to take interaction effects into account. We treat the particles again as identical two-level atoms and assume fixed particle positions $\vec{r}_i$ with equal atomic transition dipole orientations and amplitudes for all particles, $\vec{\mu}_i = \vec{\mu}$ for all i. Following the derivation in [14, 15] we find two contributions of the collective effects to our system. As mentioned in section 2.2.2 we need to take collective decay, instead of independent, of the two-level atoms into account. The rates in 2.27 are given by

$$\Gamma_{ij} = \frac{3}{2}\Gamma\Big[(1-\cos^2\theta)\frac{\sin(k_a r_{ij})}{k_a r_{ij}} + (1-3\cos^2\theta)\left(\frac{\cos(k_a r_{ij})}{(k_a r_{ij})^2} - \frac{\sin(k_a r_{ij})}{(k_a r_{ij})^3}\right)\Big], \tag{2.29}$$

with $r_{ij} = |\vec{r}_i - \vec{r}_j|$ the absolute value of the position vector of particle i and j and θ the angel between the dipole moment and the distance vector.

The other contribution is the coherent dipole-dipole coupling, which is an additional part to the Hamiltonian 2.13, it is given by the expression

$$H_{\text{dd}} = \hbar\sum_{i\neq j}\Omega_{ij}\sigma_i^+\sigma_j^-, \tag{2.30}$$

with

$$\Omega_{ij} = -\frac{3}{4}\Gamma\Big[(1-\cos^2\theta)\frac{\cos(k_a r_{ij})}{k_a r_{ij}} - (1-3\cos^2\theta)\left(\frac{\sin(k_a r_{ij})}{(k_a r_{ij})^2} + \frac{\cos(k_a r_{ij})}{(k_a r_{ij})^3}\right)\Big]. \tag{2.31}$$

The Hamiltonian H_{dd} describes the coherent energy exchange between the atoms via dipole-dipole interaction.

In our model all dipoles are perpendicular to the distance vector between the particles, this means $\theta = \pi/2$. Figure 2.3 shows Γ_{ij} and Ω_{ij} for this configuration as a function of the distance r_{ij}. Notice, that as expected, for widely separated atoms we reach the case of independent atoms. This means for $r_{ij} \to \infty$, $\Omega_{ij} \to 0$ and $\Gamma_{ij} \to \delta_{ij}\Gamma$.

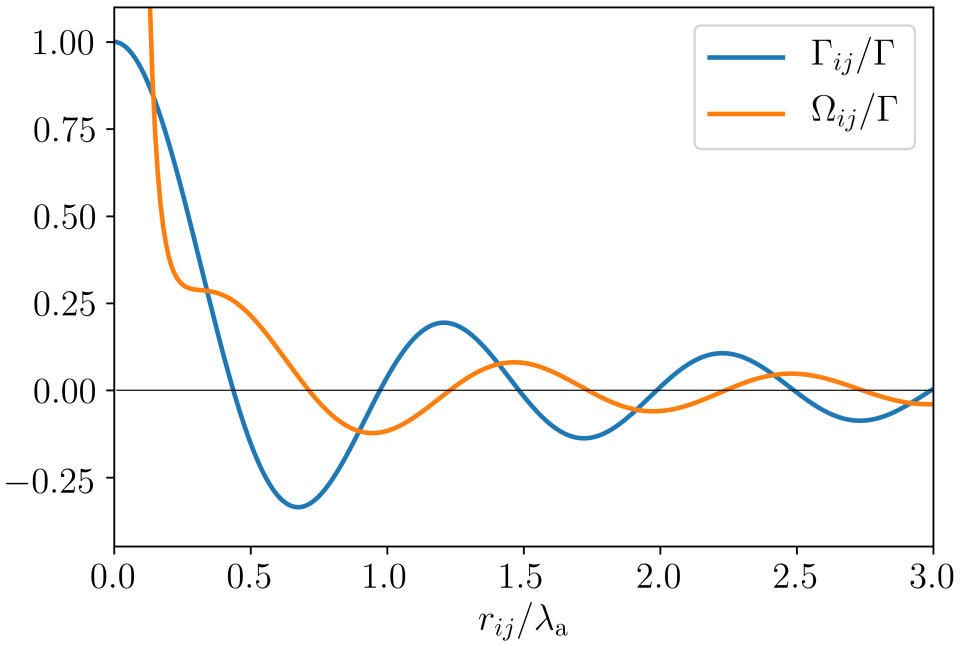

Figure 2.3.: *Collective decay rates* Γ_{ij} *and coherent dipole-dipole coupling* Ω_{ij} *as a function of* r_{ij}. $\theta = \pi/2$, Γ_{ij} and Ω_{ij} are plotted in units of Γ and the distance of the atoms is in units of λ_a. For $r_{ij}/\lambda_a \to 0$: $\Omega_{ij} \to \infty$ and $\Gamma_{ij} \to \Gamma$.

2.4. Semi-Classical Time Evolution

In this section we want to take motion of our particles into account. As a first step to do this we add classical degrees of freedom for the position and the momentum of the particles and calculate the dynamics of these variables via the Ehrenfest-theorem [16]

$$\frac{d}{dt}\langle \hat{O} \rangle = \frac{i}{\hbar}\langle [H, \hat{O}] \rangle + \langle \frac{\partial \hat{O}}{\partial t} \rangle , \tag{2.32}$$

with $\hat{O}$ an arbitrary operator in the same Hilbertspace as the Hamiltonian H. In our case we get $2N$ coupled differential equations for the particles position and momentum operator, $\hat{r}_i$ and $\hat{p}_i$ respectively. For a Hamiltonian of the form

$$H = H_0 + V(\hat{r}_i) + \frac{\hat{p}_i^2}{2m} \tag{2.33}$$

one obtains, by use of the notation $r_i = \langle \hat{r}_i \rangle$ and $p_i = \langle \hat{p}_i \rangle$,

$$\frac{d}{dt} r_i = \frac{i}{\hbar} \langle [H, \hat{r}_i] \rangle = \frac{p_i}{m} \tag{2.34}$$

and

$$\frac{d}{dt} p_i = \frac{i}{\hbar} \langle [H, \hat{p}_i] \rangle \approx -\frac{d}{dr_i} V(r_i). \tag{2.35}$$

The operators $\hat{r}_i$ and $\hat{p}_i$ are not explicitly time-dependent therefore the partial time derivative in 2.32 is zero. The expression on the right-hand side of (2.35) describes the force on the i-th particle. We use here the approximation that the expectation value of the position depending force is almost equal to the force depending on the expectation value of the position

$$\langle F(\hat{r}_i) \rangle \approx F(\langle \hat{r}_i \rangle). \tag{2.36}$$

To set up dimensionless equations for the numerical calculations the definition of the recoil frequency

$$\omega_{\mathrm{r}} = \frac{\hbar k_{\mathrm{a}}^2}{2m} \tag{2.37}$$

will later be useful.

2.5. Cavity Cooling

The principle of our cooling and trapping is cavity cooling. In this section we briefly explain the idea behind cavity cooling and mention its key properties for a setup with incoherently pumped atoms [8, 9, 17]. The task of a cooling process is always to reduce the kinetic energy of the particles. For cavity cooling the principle mechanism is always the same. Kinetic energy of the particles is shuffled to the cavity field and the cavity field dissipates it in a controlled manner through the cavity loss channel. This can be done in two different ways, either you pump the atoms or you pump the cavity mode, a combined process using both processes is also possible.

We will focus on the method relevant to our case, which is the pumping of the atoms in the bad cavity regime. The procedure can be as follows: We pump the atoms transversally to the cavity axis almost on resonance, the resonance frequency of the cavity mode is prepared to be higher than the atomic transition frequency $\Delta = \omega_{\mathrm{c}} - \omega_{\mathrm{a}} > 0$, this means the cavity field mode is blue detuned with respect to the atomic transition.

If the coupling of the atoms to the cavity field is significant smaller than the cavity loss rate, then it is probable that the atom scatters a photon into the cavity and the photon is lost immediately through the cavity loss channel. Since atoms inside a cavity favour to scatter photons near the cavity resonance frequency into the cavity, this provokes an

energy upshift of the emitted photon. This energy difference can be provided by the kinetic energy of the atoms, implying that every photon scattered from an atom into the cavity reduces the kinetic energy of the atom. With the coupling g small compared to the cavity loss rate κ the problem simplifies, since absorption of a cavity photon leads to heating of the atom.

An example for the time evolution of the relative kinetic energy (4.2) and the position of such a coherently pumped two-level atom inside a cavity is shown in figure 2.4. We calculate numerically the time evolution for this problem in a semi-classical approximation, the spacial coordinates are restricted to one dimension along the cavity axis. The Hamiltonian of the system in the rotating frame of the pump laser with frequency ω_l is given by

$$H = -\hbar\Delta_\mathrm{c} a^\dagger a - \hbar\Delta_\mathrm{a}\sigma^+\sigma^- + \hbar g(r)[a\sigma^+ + a^\dagger\sigma^-] + \hbar\Omega_\mathrm{R}(\sigma^+ + \sigma^-), \tag{2.38}$$

with $\Delta_\mathrm{c} = \omega_\mathrm{l} - \omega_\mathrm{c}$ and $\Delta_\mathrm{a} = \omega_\mathrm{l} - \omega_\mathrm{a}$. The last part of the Hamiltonian describes the coherent pump, with the Rabi-frequency Ω_R. The Liouvillian consists out of the cavity loss channel (2.24) and the spontaneous emission of the single two-level atom (2.26)

$$\mathcal{L} = \mathcal{L}_\mathrm{cav} + \mathcal{L}_\mathrm{sp}. \tag{2.39}$$

The coupled differential equations of motion for the atoms position and momentum can be calculated with the Ehrenfest-theorem 2.4, we obtain

$$\frac{d}{dt}r = \frac{p}{m} \tag{2.40}$$

and

$$\frac{d}{dt}p = -\frac{d}{dr}g(r)\hbar\left\langle a\sigma^+ + a^\dagger\sigma^-\right\rangle. \tag{2.41}$$

Since we are only looking at a system with one atom we do not get any collective effects. In chapter 3 we show the procedure to gain the equations for the time evolution for a similar model in more detail, therefore we disclaim to do this here. In our model we do not pump the two-level atoms coherent but apply, as mentioned in section 2.2.3, an incoherent pump to the atoms. Therefore, instead of performing Rabi-oscillations the atoms just get inverted to the excited state. This means for a sufficiently high pump rate R the scattering of a photon into the cavity happens more frequently compared to the coherent pump and absorption of a cavity photon is less probable, since the atoms have a higher probability of being in the excited state. Nevertheless the fundamental mechanism of the cooling process in our model is the same as for the example described above. Fortunately, inverted atoms in a blue-detuned cavity are high field seekers. This is an essential feature for a simultaneously lasing and cooling process, since the atoms locate at positions close to the maximal atom-cavity coupling.

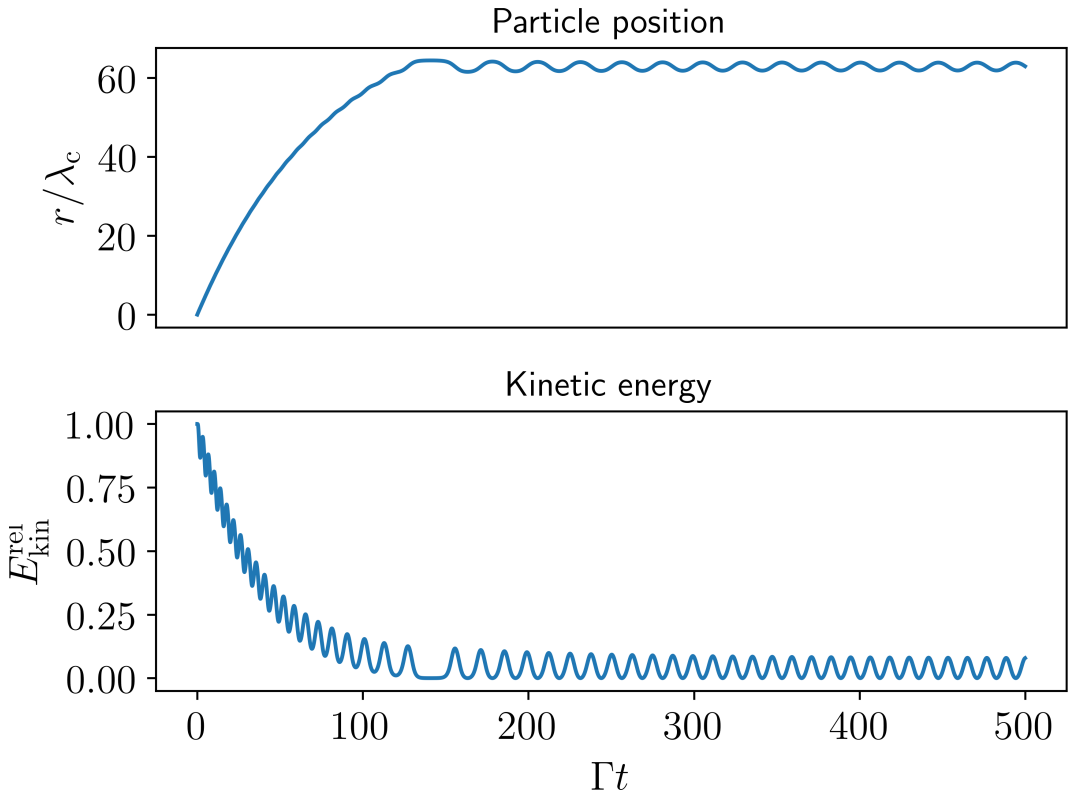

Figure 2.4.: *Cavity cooling for a single two-level atom.* You can see that the atom gets trapped at approximately $r = 60\lambda_c$ (top) and the relative kinetic energy decreases (bottom) as supposed for a cooling process. The parameters used to produce these plots are $\omega_r = 0.1\Gamma$, $\Delta_c = -4\Gamma$, $\Delta_a = -0.5\Gamma$, $\xi = 1.5\Gamma$, $g = 4\Gamma$ and $\kappa = 15\Gamma$. The atom starts at the position $r = 0$, with the momentum $p = 5\hbar k_a$ and it is in the ground state. There are no photons inside the cavity initially.

2.6. Laser Theory

To describe the principle of a laser [18] we want to take the three fundamental processes between the energy levels of the two-level atom into account, namely spontaneous emission, absorption and stimulated emission. As the name laser (light amplification by stimulated emission of radiation) quotes, stimulated emission is used to amplify radiation. Unfortunately, considering only the three processes of a two-level atom from above is not sufficient to construct a laser. In a simplified picture this can be explained by the following: Absorption occurs when a photon hits an atom in the ground state, stimulated emission is present when a photon hits an atom in the excited state and spontaneous emission can only happen when the atom is in the excited state, see figure 2.5. The only possibility to excite a two-level atom is with a coherent pump, but applying a coherent pump on the atoms can populate the exited state on time average maximally to 50%. Due to spontaneous emission this population reduces. As a consequence absorption of photons happens more often as stimulated emission, since the atoms are with higher probability in the ground state rather than in the excited state. This leads to a reduction instead of an increase of the cavity photon number. Therefore population inversion needs to be reached by some process, such as the incoherent pump mechanism described in section 2.2.3. To achieve this we need to consider at least three suitable energy levels instead of two. A mathematical description of this is given by the Einstein rate equation.

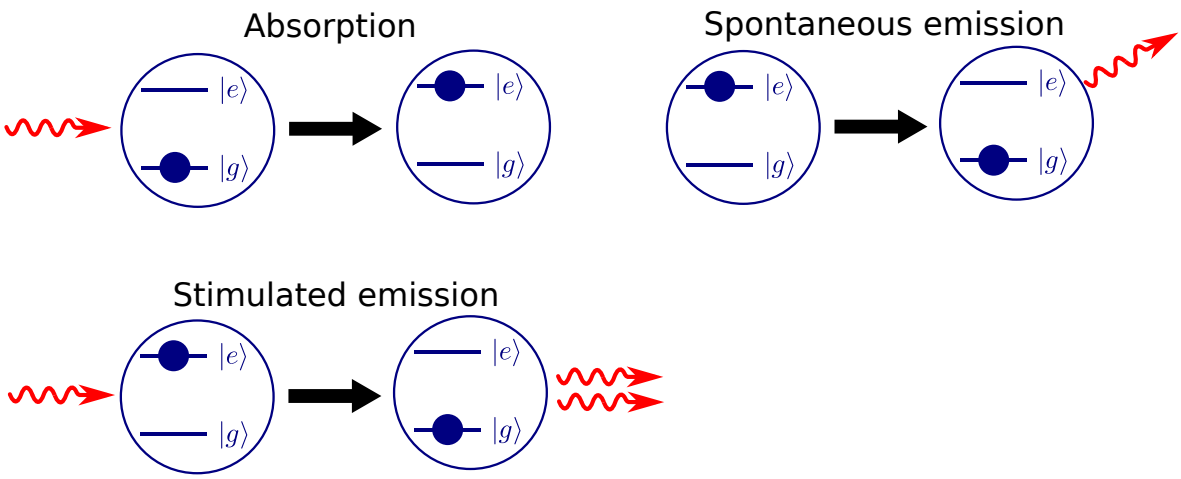

Figure 2.5.: *Sketch of absorption, stimulated emission and spontaneous emission.* Stimulate emission produces a copy of the incoming photon. Spontaneous emission emits a photon in some random direction.

The operation of a laser can be described as follows: Population inversion of the atoms is gained with an incoherent pump, such that most of the atoms are in the excited state. Now one photon is needed for the ignition of the process, for example from spontaneous emission of an excited atom. This photon stimulates then the decay of a second atom, producing a second identical photon. This yields a chain reaction of stimulated photon emissions from the excited atoms. Putting the atoms between two mirrors leads to several round trips of the photons and thus to multiple interactions with the atoms. The atoms which are in the ground state after the stimulated emission get again excited due to the incoherent pump. The photons leak continuously through one of the mirrors, providing the laser light. This schematic laser process is depicted in figure 2.6. As noted in section 2.2.3 we do not care about the internal level structure of the atom, but rather presume that a suitable atom exists which can be described mathematically in a good approximation with the incoherent pump Liouvillian (2.28).

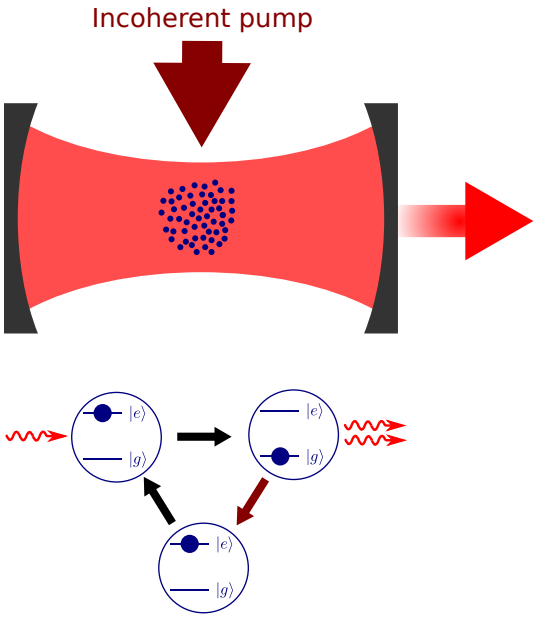

Figure 2.6.: *Principle of the laser mechanism.* You can see the laser setup (top) including the mirrors, the incoherent pump, the light field and the atoms between the mirrors. As well as the fundamental processes of the laser (bottom).

Now we provide the most important concepts needed to describe our laser properties. We mentioned in the introduction that the task of a superradiant laser is to generate laser light with a narrow linewidth. To analyze the spectrum for different parameters we need to calculate it, this can be done with the Wiener-Khintchine theorem [11]

$$S(\omega) = 2\Re\left\{\int_0^\infty d\tau e^{-i\omega\tau} g^{(1)}(\tau)\right\}. \tag{2.42}$$

The theorem states that the spectrum of a light field is given by the Fourier transform of the first order correlation function

$$g^{(1)}(\tau) = \langle a^\dagger(\tau) a(0)\rangle\,. \tag{2.43}$$

Another important propertie of a laser is the second order intensity correlation function with zero time delay [19]

$$g^{(2)}(0) = \frac{\langle a^\dagger a^\dagger a a\rangle}{\langle a^\dagger a\rangle^2}, \tag{2.44}$$

which gives knowledge of the degree of coherence of a light field. For $g^{(2)}(0) = 1$ we have coherent, for $g^{(2)}(0) > 1$ bunched and for $g^{(2)}(0) < 1$ antibunched light. The photon number inside the cavity is given by

$$n = \langle a^\dagger a \rangle \tag{2.45}$$

and the total population of the exited states by

$$p_\mathrm{e} = \sum_{i=1}^{N} \langle \sigma_i^+ \sigma_i^- \rangle \,. \tag{2.46}$$

Population inversion is present if $p_\mathrm{e} > N/2$.

Chapter 3.

Semi-Classical Model of Superradiant Lasing

With the concepts provided in chapter 2 we set up a mathematical description of our model. The model is composed of the following parts.

We consider N identical two-level atoms inside a cavity, moving along the cavity axis. Each two-level atom has a transition frequency ω_a and a transition dipole moment $\vec{\mu}$. The directions of these dipole moments are the same for all particles, parallel to each other and perpendicular to the cavity axis. The dipoles align in this way due to the light field inside the cavity. We assume that only one longitudinal light mode in the cavity is relevant, the frequency of this mode is denoted by ω_c. The spatial mode function is proportional to $\cos(k_\mathrm{c} r)$, with the wave vector k_c and the position r along the cavity axis. The atoms couple to the cavity field mode via the well-known Tavis-Cummings interaction with an atomic position-dependent coupling $g(r_i)$. Given that the atoms are closely spaced, we need to take coherent dipole-dipole energy exchange (Ω_{ij}) and collective spontaneous emission (Γ_{ij}) into account. Furthermore we create a population inversion of the two-level atoms by an individual transverse incoherent pump with pump rate R. The loss of photons through the cavity mirrors occurs at rate κ. The model specified in this paragraph is depicted in figure 3.1.

Now we write down the above model mathematically, the energy conserving parts are included in the Hamiltonian H and the dissipative processes in the Liouvillian $\mathcal{L}$. The resulting Hamiltonian without a semi-classical approximation is

$$\begin{aligned} H = {} & \hbar\omega_\mathrm{c} a^\dagger a + \hbar\omega_\mathrm{a} \sum_{i=1}^{N} \sigma_i^+ \sigma_i^- + \hbar \sum_{i=1}^{N} g(\hat{r}_i)[a\sigma_i^+ + a^\dagger \sigma_i^-] \\ & + \hbar \sum_{i \neq j} \Omega(\hat{r}_{ij}) \sigma_i^+ \sigma_j^- + \sum_{i=1}^{N} \frac{\hat{p}_i^2}{2m}. \end{aligned} \tag{3.1}$$

It consists of the Hamiltonian of the intra-cavity light field (2.3), the atomic excitation (2.9), the interaction between the atoms and the cavity light field (2.10), the coherent dipole-dipole interaction (2.30) and the total kinetic energy of the particles, summed

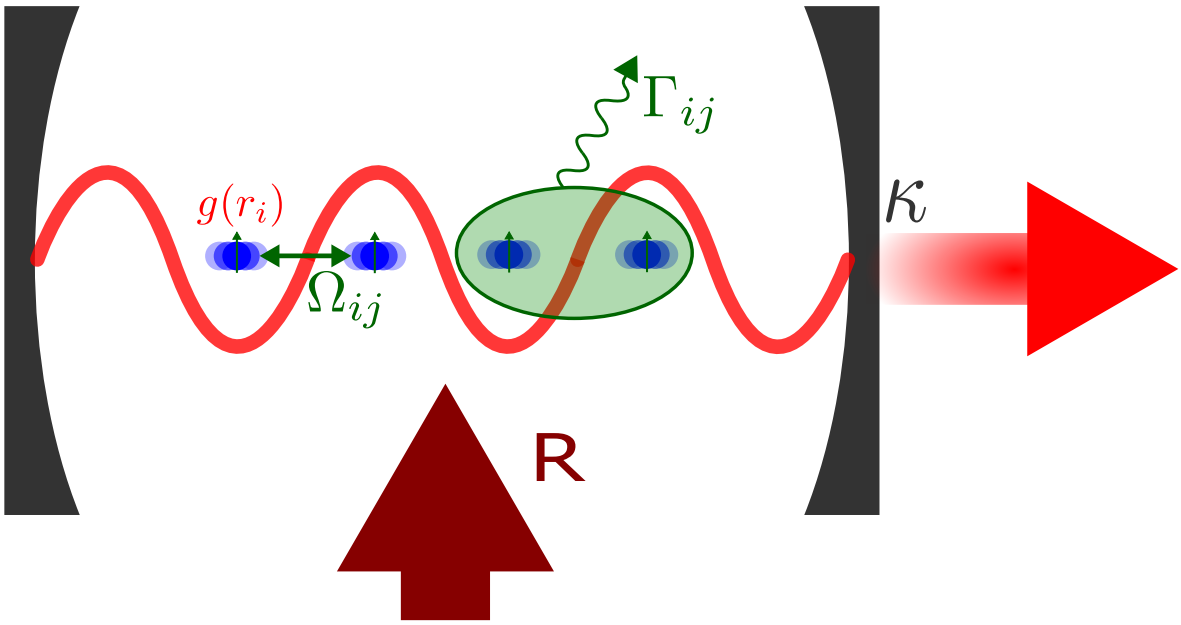

Figure 3.1.: *Schematic showing the system under consideration.* We consider a linear chain of two-level atoms coupled to the cavity mode with $g(r_i)$. Dipole-dipole coupling between the atoms Ω_{ij} and collective decay with decay rate Γ_{ij} is included as well as an independent transversal incoherent pump with pump rate R and cavity losses with loss rate κ.

up here in this order. The first three parts together are known as the Tavis-Cummings Hamiltonian (2.13). We especially indicate here that Ω_{ij} depends on the position operators $\hat{r}_i$ and $\hat{r}_j$ and not just their average values by using $\Omega(\hat{r}_{ij})$ instead.

Changing into the rotating frame of the two-level atoms, using the rotating operator as in equation 2.18, we end up with the Hamiltonian

$$H = \hbar\Delta a^\dagger a + \hbar\sum_{i=1}^{N} g(\hat{r}_i)[a\sigma_i^+ + a^\dagger\sigma_i^-] + \hbar\sum_{i\neq j}\Omega(\hat{r}_{ij})\sigma_i^+\sigma_j^- + \sum_{i=1}^{N}\frac{\hat{p}_i^2}{2m}. \tag{3.2}$$

This can easily be checked by inserting the Hamiltonian 3.1 into the rotating frame formula 2.17, as we have similarly done in section 2.1.1. There is one remaining part to show, namely $R(t)H_{\mathrm{dd}}R^\dagger(t) = H_{\mathrm{dd}}$, but this is also straight forward to calculate.

As a first step to include particle motion in the model, we approximate it within a semi-classical treatment. We apply the Ehrenfest-theorem (2.32) and the approximation (2.36) on the Hamiltonian (3.2) to gain $2N$ coupled differential equations. For the velocity of the i-th particle we obtain

$$\frac{d}{dt}r_i = \frac{i}{\hbar}\langle[H,\hat{r}_i]\rangle = \frac{p_i}{m} \tag{3.3}$$

and for the momentum change

$$\frac{d}{dt}p_i \approx -\frac{d}{dr_i}\left[\hbar g(r_i)\left\langle a\sigma_i^+ + a^\dagger\sigma_i^-\right\rangle + \hbar\sum_{i\neq j}\Omega_{ij}\left\langle\sigma_i^+\sigma_j^-\right\rangle\right]. \tag{3.4}$$

The semi-classical model is then completely described with these $2N$ coupled differential equations, the Hamiltonian

$$H = \hbar\Delta a^\dagger a + \hbar\sum_{i=1}^{N} g(r_i)[a\sigma_i^+ + a^\dagger\sigma_i^-] + \hbar\sum_{i\neq j}\Omega_{ij}\sigma_i^+\sigma_j^- \tag{3.5}$$

and the Liouvillian composed of the three summands

$$\mathcal{L} = \mathcal{L}_{\text{cav}} + \mathcal{L}_{\text{cd}} + \mathcal{L}_{\text{pump}}, \tag{3.6}$$

the cavity loss channel (2.24), the collective atomic decay (2.27) and the transversal incoherent pump (2.28). The Liouvillian does not change in the semi-classical approximation, only the atomic positions in the expression for the collective decay become real values instead of operators. Since we do not take the recoil arising from spontaneous emission into account, it is sufficient to use the Ehrenfest-theorem to calculate the semi-classical equations of motion. Therefore we do not have any direct contributions from the dissipative processes to the particles equations of motions.

Chapter 4.

Lasing, Cooling and Trapping

In this chapter we investigate the stability of the laser system described above during lasing operation. We find that for properly chosen parameters the atoms are cooled and even trapped within the potential created by the laser light in the cavity mode. We carry out a lot of parameter scans in different regimes to analyze the cooling properties of the system.

4.1. Semi-Classical description of Cooling and Trapping

Due to the exponential scaling of the atomic Hilbert space dimension with the number of atoms numerical methods are limited. We thus restrict ourselves to treating a system of few atoms which nevertheless exhibits collective behaviour. The procedure is always the same: We look at a system with three atoms inside the cavity. These atoms are placed initially $\lambda_c/2$ apart at positions where the generated intracavity light forces are zero, this means e.g. at 0, $\lambda_c/2$ and λ_c. The atoms start in the ground state and there are no photons inside the cavity. The set of initial momenta p_0 depends on the chosen recoil frequency, which we specify later. To generate some comparable guiding values of the cooling process we study the time evolution of the particles positions and their kinetic energy

$$E_{\mathrm{kin}}(t) = \sum_{i=1}^{N} \frac{p_i^2(t)}{2m}. \tag{4.1}$$

As observable we choose the ratio between the current and initial kinetic energy

$$E_{\mathrm{kin}}^{\mathrm{rel}}(t) = \frac{E_{\mathrm{kin}}(t)}{E_{\mathrm{kin}}(t=0)}. \tag{4.2}$$

Due to the fact that the kinetic energy is oscillating very rapidly on the time scale of the cooling process, the information we seek is not simply given by $E_{\mathrm{kin}}^{\mathrm{rel}}(t = t_{\mathrm{end}})$. Therefore we introduce an average relative kinetic energy $\bar{E}_{\mathrm{kin}}^{\mathrm{rel}}$ over one oscillation period, which is obtained by just taking the midpoints between two adjacent extrema of the relative kinetic energy, see figure 4.1.

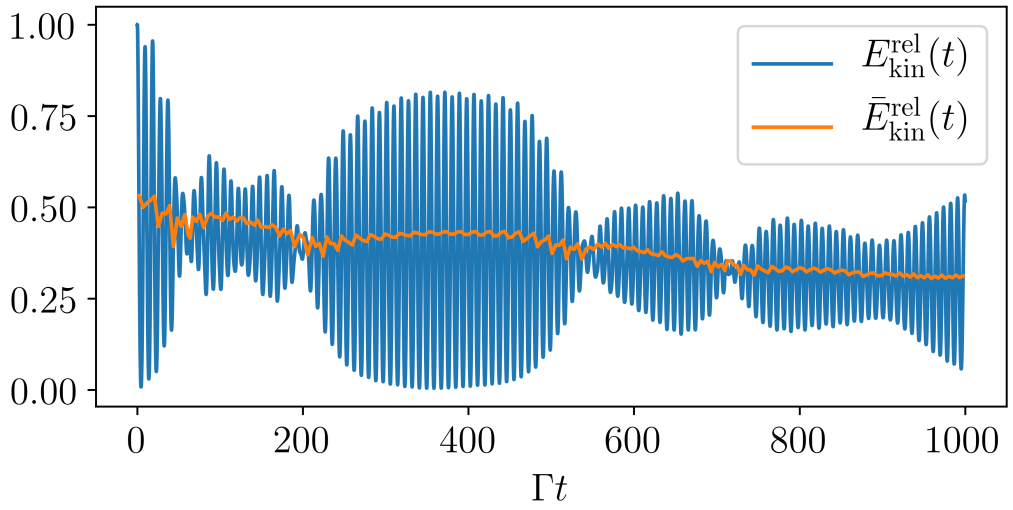

Figure 4.1.: *Method to obtain the average relative kinetic energy loss.* As the oscillation of the relative kinetic energy (blue) is too fast to give some reliable guiding value, we average it over one period (orange). We show the time evolution from $\Gamma t = 0$ to 1000. The parameters are $\omega_{\mathrm{r}} = 0.1\Gamma$, $\Delta = 5\Gamma$, $g = 5\Gamma$, $\kappa = 20\Gamma$, $R = 8\Gamma$ and $p_0 = [1.7, -1.6, 1.5]\hbar k_a$.

The parameter we use to characterize cooling or heating is then

$$\bar{E}^{\mathrm{rel}}_{\mathrm{kin}} = \frac{\bar{E}^{\mathrm{rel}}_{\mathrm{kin}}(t_{\mathrm{end}})}{\bar{E}^{\mathrm{rel}}_{\mathrm{kin}}(t=0)}. \tag{4.3}$$

Simply put, it is just the last point of the orange line divided by the first point of the orange line in figure 4.1

The method described above will be used to characterize the cooling process and find regimes of stable operation. We define what we mean by stable. The light field inside the cavity produces a potential which is felt by the atoms. For correctly chosen parameters this potential can lead to trapping of the atoms. The periodicity of this potential is $\lambda_{\mathrm{c}}/2$, given by (2.10), which means that the n-th trapping potential has a range from $-1/4 + n/2$ to $1/4 + n/2$. We want the atoms stay in the range of their initial position. If this is the case for the whole time evolution, we call the configuration stable. In figure 4.2 you can see a typical stable configuration.

In comparison, a configuration is denoted as unstable if at least one atom leaves its initial trap. We distinguish between two unstable cases, either $\bar{E}^{\mathrm{rel}}_{\mathrm{kin}} > 1$ or $\bar{E}^{\mathrm{rel}}_{\mathrm{kin}} < 1$. The second case, $\bar{E}^{\mathrm{rel}}_{\mathrm{kin}} < 1$, means that the system might cool the atoms, but the trap is not strong enough to keep them localized at all times. Although the particles may get trapped somewhere, we do not calculate the kinetic energy, because we want to take collective effects into account and this is not provided for widely separated atoms.

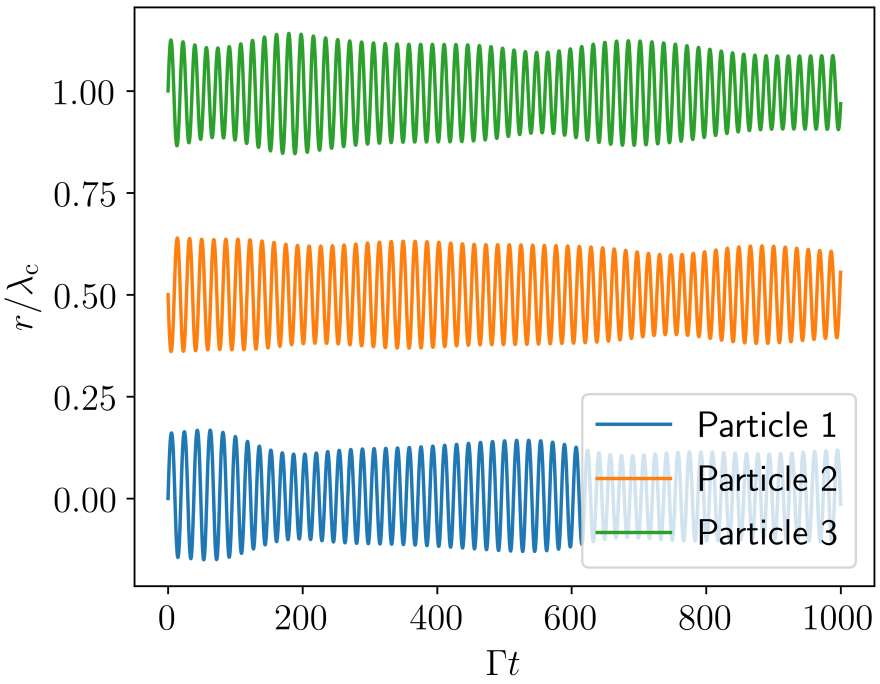

Figure 4.2.: *Stable configuration of atoms.* You can see the trajectories of three atoms inside the cavity from $\Gamma t = 0$ to 1000. We call these trajectories stable, because the atoms stay in their initial trap. The parameters are the same as in figure 4.1.

This case is denoted as metastable configuration, see figure 4.3. In the scan plots these areas will have the color black. Moreover, every value of $E_{\text{kin}}^{\text{rel}}$ above 1.0 corresponds to heating and is artificially fixed to 1.0 as these are points of little interest.

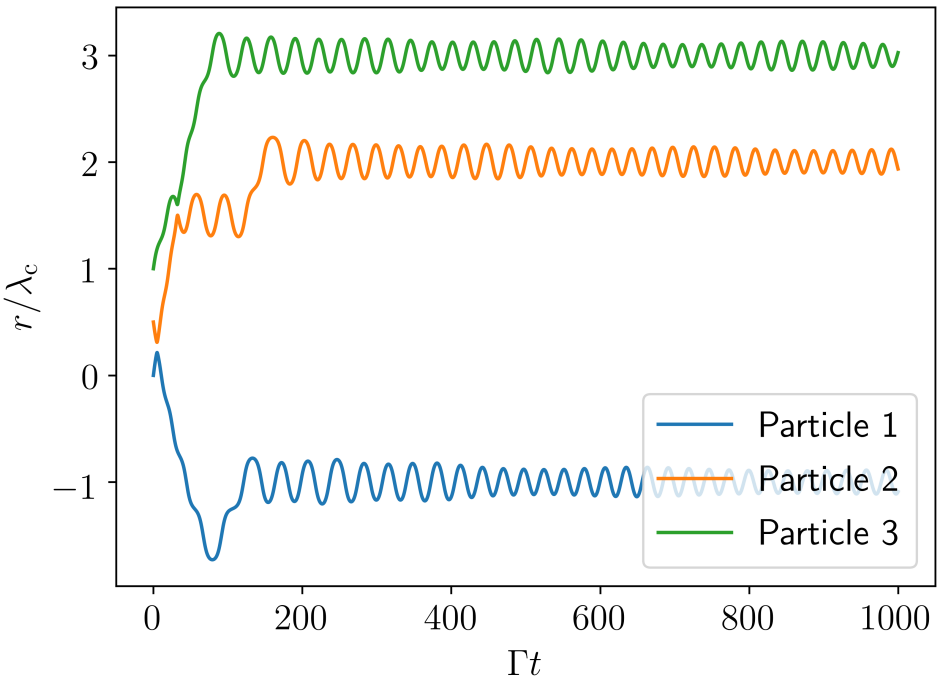

Figure 4.3.: *Metastable configuration of atoms.* You can see the trajectories of three atoms inside the cavity from $\Gamma t = 0$ to 1000. We call these trajectories metastable, because the atoms do not stay in their initial trap, but they get cooled and then trapped at other positions. All parameters are the same as for the stable case, except g is changed from 5Γ to 3Γ.

4.2. Results

Let us now scan over the parameters which are easiest to tune experimentally, using the method described above. We perform this procedure for three different recoil frequencies ω_r. The values of the parameters not changed in the scan, are given in the figure caption. For numerical calculations one needs to confine the Hilbertspace of the photons. We set the maximal photon number to three, which is enough because we have average photon numbers below one around 0.3. We also checked that the results do not change for higher maximal photon numbers. The three initial sets of momenta for the different ω_r are:

- $\omega_r = 0.1\Gamma$: $[1.7, -1.6, 1.5]\hbar k_a$, $[1.7, 1.5, 1.6]\hbar k_a$ and $[1.6, 1.5, -1.7]\hbar k_a$
- $\omega_r = 1.0\Gamma$: $[0.55, -0.5, 0.45]\hbar k_a$, $[0.55, 0.45, 0.5]\hbar k_a$ and $[0.5, 0.45, -0.55]\hbar k_a$
- $\omega_r = 10.0\Gamma$: $[0.14, -0.13, 0.12]\hbar k_a$, $[0.14, 0.12, 0.13]\hbar k_a$ and $[0.13, 0.12, -0.14]\hbar k_a$

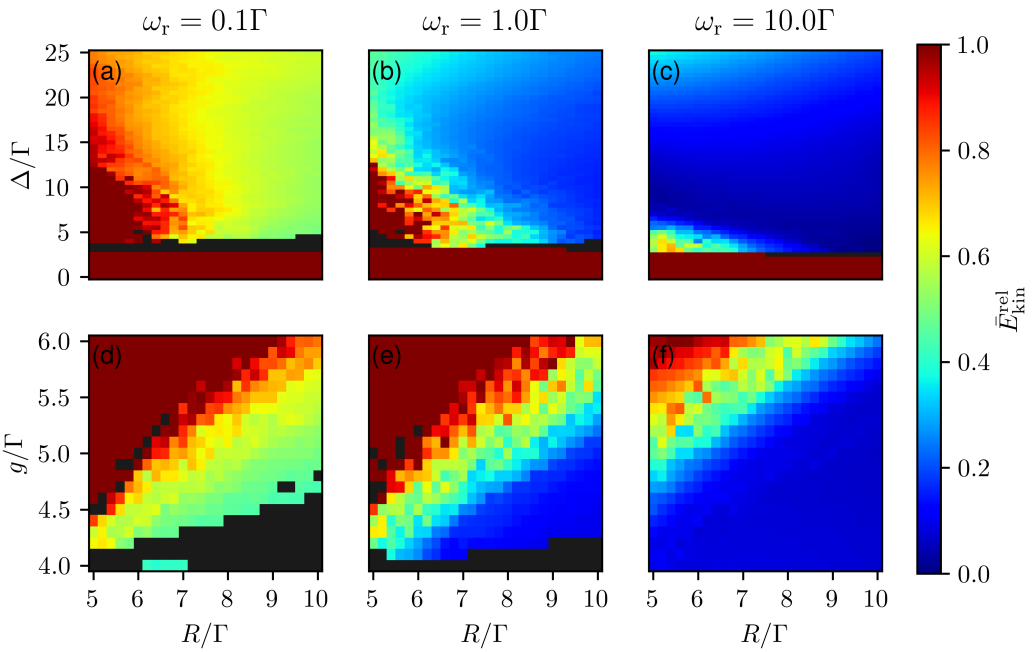

Figure 4.4.: *Scans of the final kinetic energy* $\bar{E}^{\mathrm{rel}}_{kin}$. You can see a scan over Δ and R in (a)-(c) for different ω_r and the same for g and R in (d)-(f). The remaining parameters are $\Delta = 5\Gamma$, $g = 5\Gamma$, $\kappa = 20\Gamma$ and $t_{\mathrm{end}} = 1000/\Gamma$. The black areas show unstable configurations with $\bar{E}^{\mathrm{rel}}_{\mathrm{kin}} < 1$ (metastable) and the dark red areas represent $\bar{E}^{\mathrm{rel}}_{\mathrm{kin}} \geq 1$.

To start always with the same initial energy, the absolute values of the initial momenta are always chosen the same for a specific value of the recoil frequency, only the distribution on the particles and signs are different. This provokes clear differences in the trajectories. You can also see that we use smaller initial momenta for bigger ω_r. This is due to the fact that a bigger ω_r corresponds to a smaller particle mass, which consequently leads to higher initial kinetic energy, for equal initial momenta. For too high initial kinetic energies the trap is not strong enough to keep the particles localized. We chose the initial momenta such that most of the trapped particles have a maximal displacement with respect to the middle of their trap of approximately $0.2\lambda_c$. Figure 4.4 shows the final kinetic energy $\bar{E}^{\mathrm{rel}}_{\mathrm{kin}}$ (4.3) for a scan over Δ and R and over g and R for the three different ω_r.

Note, that we only consider $\Delta > 0$, which corresponds to the cavity mode being blue-detuned from the atoms. Hence, when an atom emits into the cavity mode it emits at a frequency higher than its transition frequency. Therefore, the atom has to exert energy in order to lose a photon into the cavity, which it does by losing kinetic energy. The atoms feel an effective friction force that is largest at the points where the cavity field is maximal (high-field seeking). As can be seen from the scans, there is an optimum

for the detuning where the cooling is maximal. This is similar to the maximal force in the process of Doppler cooling. The force is also proportional to the inversion of the atoms. The cooling is thus best when the atoms are pumped very strongly (large R).

Due to the fact that we have to reduce the initial momenta of particles with higher ω_r to trap them, we can say that lighter particles are harder to keep in place than heavier ones, for the same initial momenta. But if they are cold enough they are easier to cool down further (compare figure 4.4(a), (d) and (c), (f)).

Finally, as can be seen in figure 4.4(d)-(f), the coupling to the cavity mode should not be too large in order for the system to be stable and cool reliably. This can be explained by the growing probability of the atoms to absorb photons from the cavity, which causes heating. Hence, the coupling should always be well below the cavity loss rate, such that it is much more probable for a photon to leave the cavity than to be reabsorbed.

At this point we want to mention again that we describe the system in a semi-classical treatment and we neglect the recoil arising from spontaneous emission. Since the absolute values of the particles' momenta are around $\hbar k_\mathrm{a}$ we need to have a critical point of view on the cooling and trapping results, especially for the $\omega_\mathrm{r} = 1\Gamma$ and $\omega_\mathrm{r} = 10\Gamma$ cases.

4.2.1. Collective Cooling Effects

In this subsection we want to demonstrate the collective effects of the cooling process. Therefore we switch them on and off and compare the independent cooling with the collective cooling from before. For this purpose we set $\Omega_{ij} = 0$ for all i and j and $\Gamma_{ij} = \delta_{ij}\Gamma$, with δ_{ij} the Kronecker delta. This description would fit for widely separated atoms. In figure 4.5 you can see the difference between the collective and independent final kinetic energy defined by

$$\bar{E}^{\mathrm{diff}}_{\mathrm{kin}} = \bar{E}^{\mathrm{rel}}_{\mathrm{kin,coll}} - \bar{E}^{\mathrm{rel}}_{\mathrm{kin,ind}}. \tag{4.4}$$

$\bar{E}^{\mathrm{rel}}_{\mathrm{kin,coll}}$ is the same as before (4.3) and $\bar{E}^{\mathrm{rel}}_{\mathrm{kin,ind}}$ is determined in exactly the same way just for the case of independent atoms. The black areas in these scans show parameters were one case is stable and the other is not. If both are unstable or they have the same kinetic energy, then it is displayed as white.

We can see, that for initially hotter atoms ($\omega_\mathrm{r} = 0.1\Gamma$), the collective average relative kinetic energy is lower (blue areas). This is because for atoms with higher initial kinetic energy, the dipole-dipole coupling creates an additional interaction that leads to faster cooling. However, the effective potential felt by the atoms is no longer minimal at the cavity field antinodes. Hence, the overall potential minimum is shifted and raised for collectively interacting atoms as compared to independent atoms. The result is that while dipole-dipole interactions lead to faster cooling, the final temperatures reached are not as low as for independent atoms. In figure 4.5(b),(c),(e) and (f) one can see this behaviour. For $\omega_\mathrm{r} = 1.0\Gamma$ independent atoms surpass the collectively interacting atoms

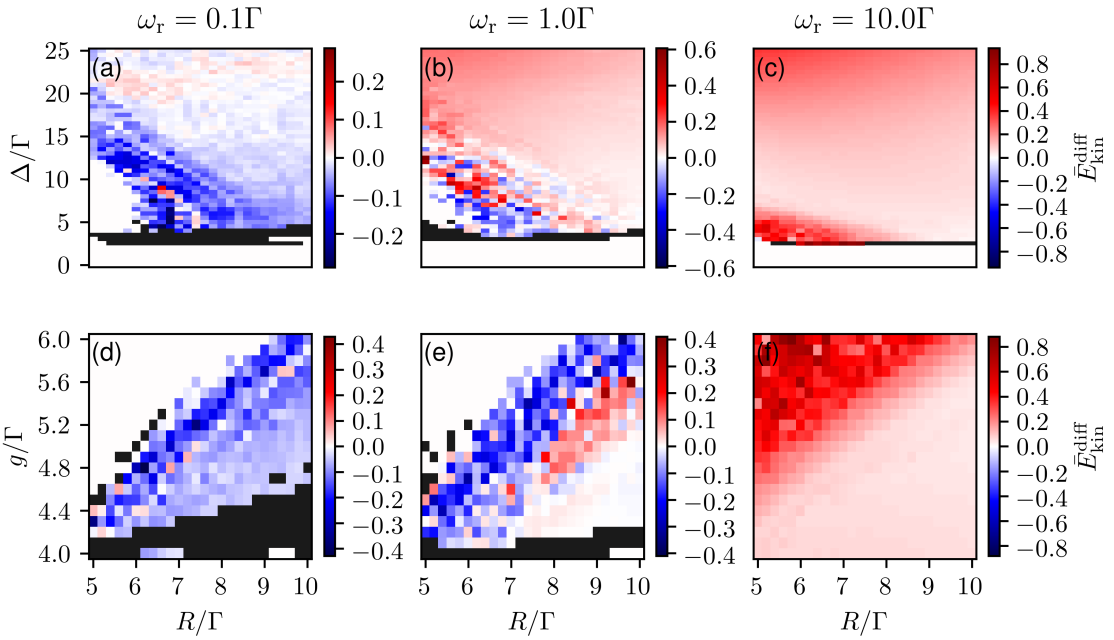

Figure 4.5.: *Difference between collective and independent final kinetic energy.* We did the same scans with the same parameters as in figure 4.4 for independent atoms ($\Omega_{ij} = 0\ \forall i, j$ and $\Gamma_{ij} = \delta_{ij}\Gamma$) and subtract these results from the collective ones. In the blue areas the collective cooling reaches smaller temperatures and in the red areas the independent cooling leads to smaller temperatures.

in terms of cooling, since they already cool down beyond the temperature possible for interacting atoms. This effect is even more dominant for $\omega_r = 10.0\Gamma$ where independent atoms are always colder (red areas). Since the above explanation is only based on three data points, we substantiate our statement by comparing the kinetic energy of collective and independent cooling for a fixed set of parameters with different initial momenta. Figure 4.6 shows $\bar{E}^{\mathrm{rel}}_{\mathrm{kin}}$ for collective and independent cooling, depending on the average initial momentum which we define by

$$\bar{p}_0 = \frac{1}{N}\sum_{i=1}^{N} |p_i|. \tag{4.5}$$

As expected the graph shows that collectively interacting atoms get cooled faster for higher initial momenta. When the atoms are cooled down further and further independent dynamics reaches lower kinetic energy, here for atoms with $\bar{p}_0 \lesssim 1\hbar k_a$. Below $\bar{p}_0 \approx 0.75\hbar k_a$ the atoms are initially too slow to be cooled further, and are heated.

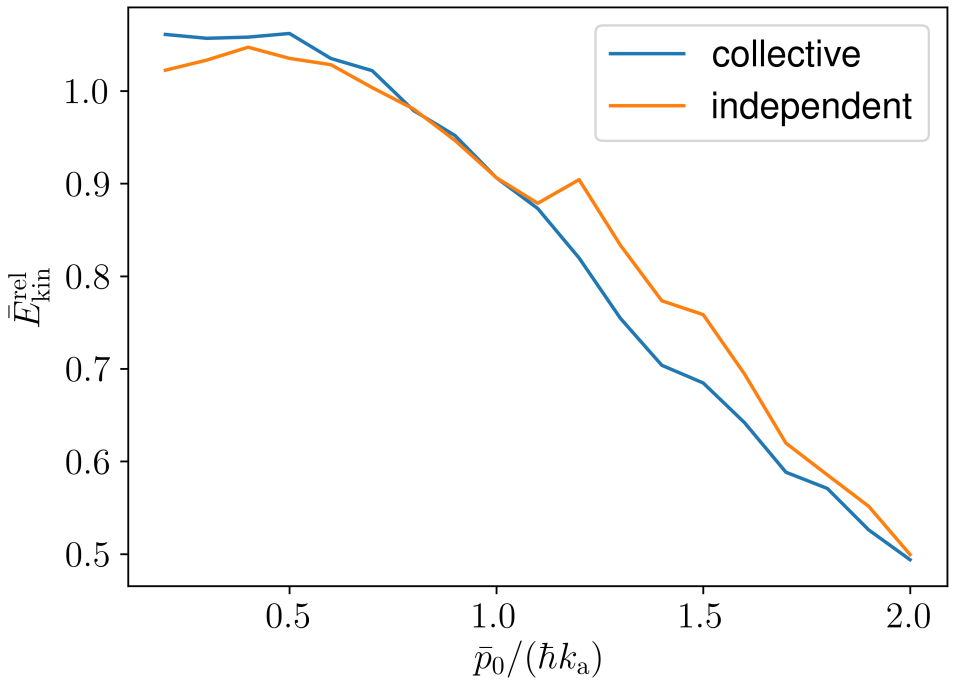

Figure 4.6.: *Comparison of collective and independent cooling for different initial momenta.* We can see a crossover of the collective and independent line at $\bar{p}_0 \approx 1\hbar k_{\mathrm{a}}$. The parameters are the same as in figure 4.1.

Chapter 5.

Laser properties

After we have established that the system shows stable lasing and trapping for a certain range of parameters, we move to analyzing the lasing properties. To this end we study the average photon number, the laser output spectrum, as well as the second order intensity correlation function. Furthermore, we look at the atomic inversion.

5.1. Method to Analyze the Laser Properties

We pick a rectangular range of stable parameters from figure 4.4. In a fully quantum mechanical model with fixed particle positions one would calculate the steady state of the system and then use this to obtain the above properties. Since we include motion in our model and it is simply not possible to cool the particles down to zero temperature (fixed particles), we will never reach the ground state, because the ongoing motion of the atoms will always lead to a change of the quantum field states. Hence we consider the density matrix at the end of a fixed long period of cooling ($t_{\text{end}} = 1000/\Gamma$) as approximation to the stationary density matrix.

To calculate the spectrum of a semi-classical system numerically we need to calculate the field correlation function $g^{(1)}(\tau)$ for a sufficiently long time τ to insert it then into the Wiener-Khinchin theorem (2.42). This can be done in the following way. We choose $\rho_0 = \rho(t = 1000/\Gamma)$ to be our initial density matrix, the first order correlation function can then be calculated by

$$g^{(1)}(\tau) = \langle a^\dagger(\tau)a(0)\rangle = tr[a^\dagger(\tau)a(0)\rho_0]. \tag{5.1}$$

To evaluate this we define the new density matrix $\rho_a = a\rho_0$ and put the time-dependence of the operator $a^\dagger$ into the density matrix ρ_a, which corresponds to a change from the Heisenberg picture to the Schrödinger picture [16]. We can then simply calculate the semi-classical time evolution of $\rho_a(\tau)$ as for $\rho(t)$ and evaluate the first order correlation function by

$$g^{(1)}(\tau) = tr[a^\dagger\rho_a(\tau)]. \tag{5.2}$$

A sufficient choice for $\tau_{\max}$ in our case is $60/\Gamma$ with a time step of $0.005/\Gamma$. $\tau_{\max}$ determines the frequency resolution and the time step is responsible for the frequency range of the spectrum. For other laser properties, n, $g^{(2)}(0)$ and p_e, we simply average from $t = 1000/\Gamma$ to $1060/\Gamma$. In contrast to a conventional laser, the spectrum is not a Lorentzian, but to extract the spectrum in terms of its linewidth and frequency offset, we use a standard least squares method to fit it with a Lorentzian distribution

$$L(\omega) = A\frac{\gamma^2}{(\omega - \delta_0)^2 + \gamma^2}, \tag{5.3}$$

with γ the half width at half maximum (HWHM), δ_0 the offset to the real atomic transition frequency ω_a and A the amplitude. An example showing good agreement of the fit and the spectrum is shown for a specific set of parameters in figure 5.1.

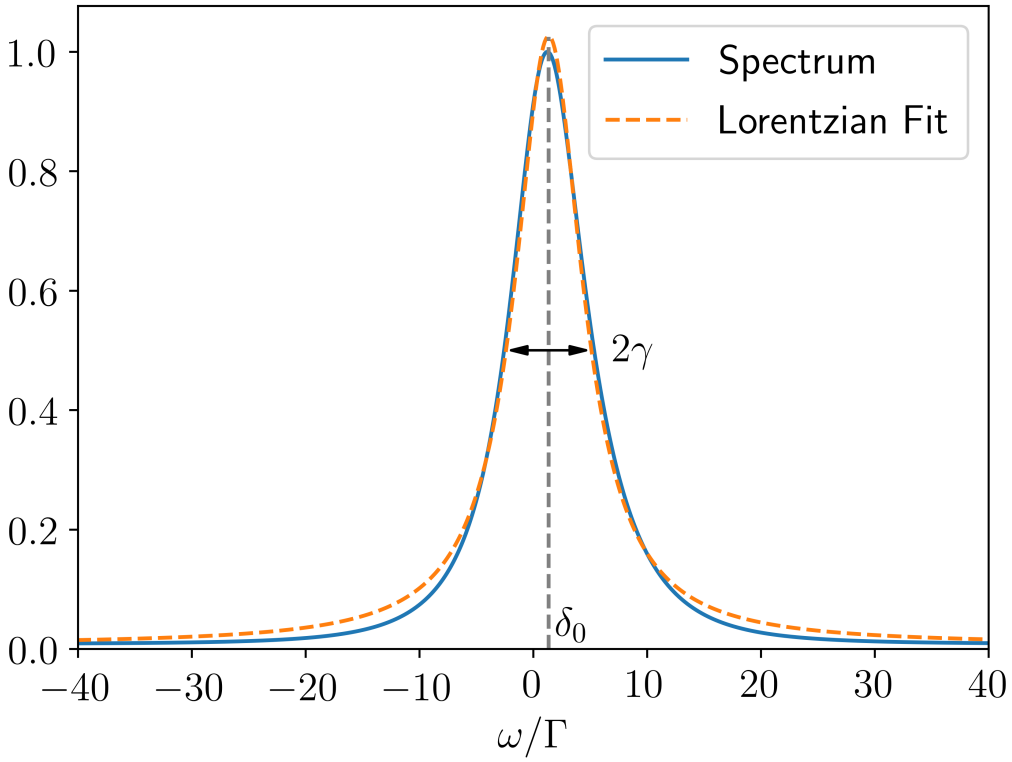

Figure 5.1.: *Lorentzian fit of the normalized spectrum.* The full width at half maximum (FWHM) in this example is $2\gamma \approx 7.5\Gamma$ and the offset $\delta_0 \approx 1.3\Gamma$. The parameters are the same as in figure 4.1.

5.2. Results

In this section we finally show the scans of the different laser properties. Here we restrict ourself to one choice of the recoil frequency, namely $\omega_r = 1.0\Gamma$, because the results are qualitatively similar for the other two cases. The dependence of the FWHM 2γ and the offset δ_0 on our chosen scan parameters is depicted in figure 5.2. The second order correlation function $g^{(2)}(0)$, the average number of intra-cavity photons n and the population of the excited state p_e is shown in figure 5.3. In figure 5.4 you can see one specific time evolution of the intra-cavity photon number n and the excited state population p_e.

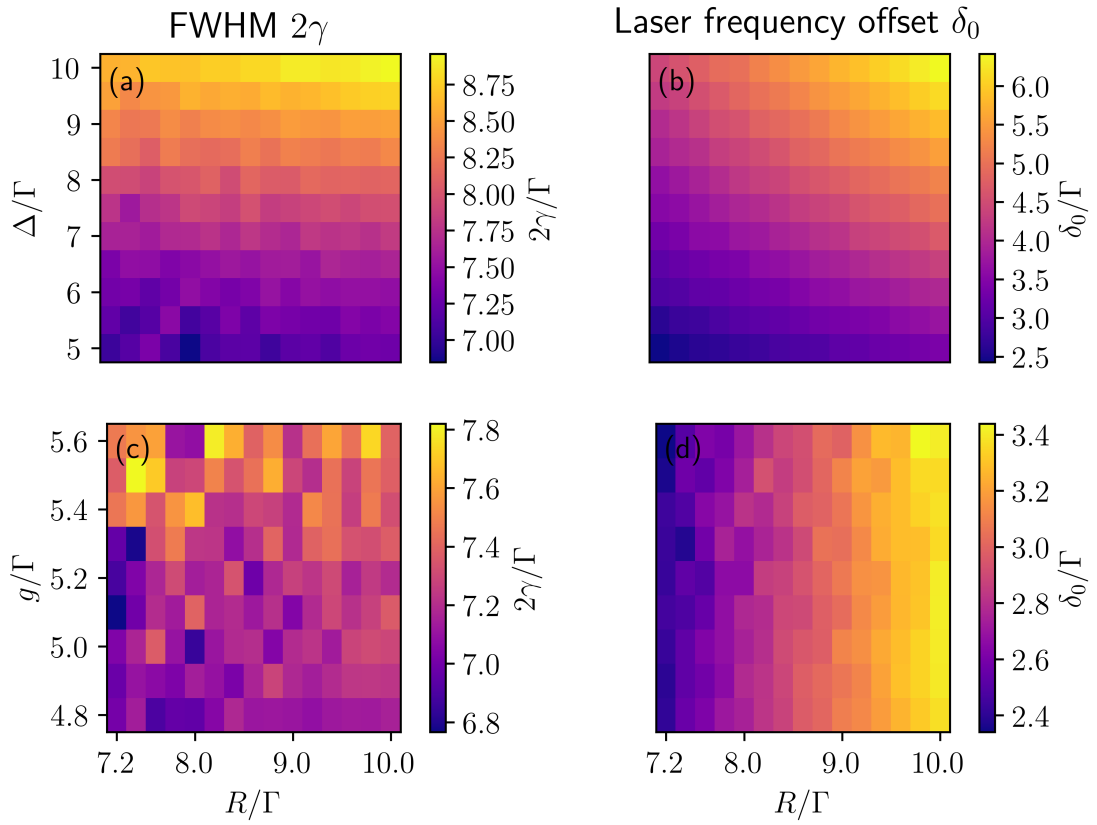

Figure 5.2.: *Dependency of the spectrum on pump strength, detuning and coupling.* You can see a scan over stable areas for the FWHM 2γ in (a) and (c) and for the offset δ_0 in (b) and (d). The parameters are the same as in figure 4.4 for $\omega_r = 1.0\Gamma$. For comparison only, the linewidth (FWHM) of the cavity without atoms is given by the cavity loss rate $\kappa = 20\Gamma$.

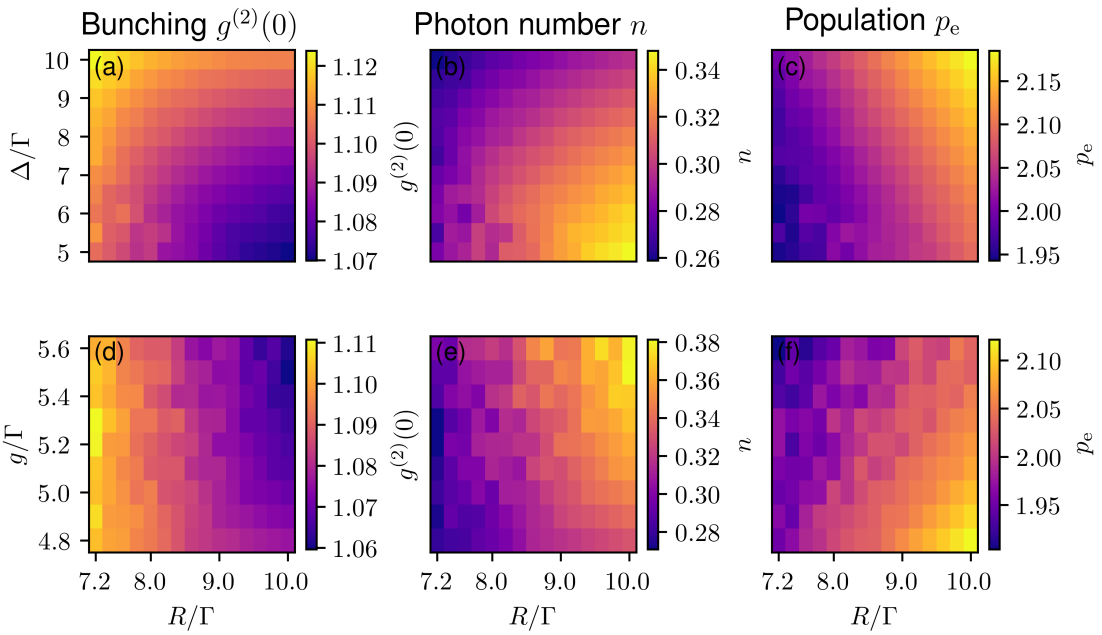

Figure 5.3.: *Dependency of the second order correlation function, the average photon number and the excited state population on pump strength, detuning and coupling.* You can see a scan over stable areas for $g^{(2)}$ in (a) and (d) for n in (b) and (e) and for p_e in (c) and (e). The parameters are the same as in figure 4.4 for $\omega_r = 1.0\Gamma$.

The central point we find in figure 5.2 is that the laser offset δ_0 is much smaller than the corresponding detuning Δ for all scan parameters, mathematically this means that the slope of the offset's dependency on the detuning is smaller than one. For a conventional laser in the good cavity regime this slope is approximately one. In our case it is roughly between 0.4 and 0.5, depending on the pump rate R. The linewidth 2γ also does not vary much with the detuning. The significance of these two features is that the spectrum of the superradiant laser depends less on cavity fluctuations than the spectrum of a normal laser, this is the expected behaviour. The values of the FWHM are relatively high, this is due to the fact that the effective atomic linewidth is given by $R + \Gamma$ and the pump rate is much higher than the spontaneous emission rate. We can also see that for all stable parameters shown in the graphs, the laser linewidth is well below the cavity linewidth $2\gamma < \kappa$. The linewidth and the offset grow with increasing pump, which implies that the best laser spectrum is created for small pump rates just above the laser threshold. The coupling does not affect the offset, but the linewidth grows with it. Considering the fact that the above mentioned values are almost the same for the three different ω_r indicates that the laser properties do not change dramatically compared to a laser with fixed particle positions as described in [7]. To confirm this statement we

calculate the spectrum, in the same manner as we did to generate figure 5.1, for fixed atom positions ($r_1 = 0$, $r_2 = \lambda_c/2$ and $r_3 = \lambda_c$). Comparing these two spectra, we only find slight differences, the plotted lines almost overlap.

The most significant feature of figure 5.3 is that we always have less than one photon on average inside the cavity. The figure also shows that the most photons are created and the field is most coherent ($g^{(2)}(0) = 1$) for small detunings and large pump strengths. The population of the excited state is of course higher for a larger pump strength and smaller coupling. However, the important point is that the atoms are always inverted ($p_e > N/2$), which is needed for lasing. Hence we see that the parameters where cooling is ideal do not coincide with optimal laser properties. For an efficient cooling process we need e.g. a big enough detuning, whereas the laser properties are best for small detuning. We therefore conclude that there is a certain trade-off between the ideal cooling and lasing regimes.

In figure 5.4 we can see that the photon number and the excited state population increase almost instantaneously. This is true for fixed and moving atoms. Due to this feature it is possible to trap atoms which are in the ground state at the beginning in a cavity with initially no photons inside. The maxima and minima population and photon number are exactly opposite. As an atom gets excited by the absorption of a photon or deexcited by the emission of a photon, we expect this behaviour. For fixed atom positions both observables immediately reach their steady state, we can see that the value for the photon number is a upper bound for the case of moving atoms, and the value for the excited state population is a lower bound. This is due to the fact, that the atoms are placed at positions where the coupling to the cavity field is maximal.

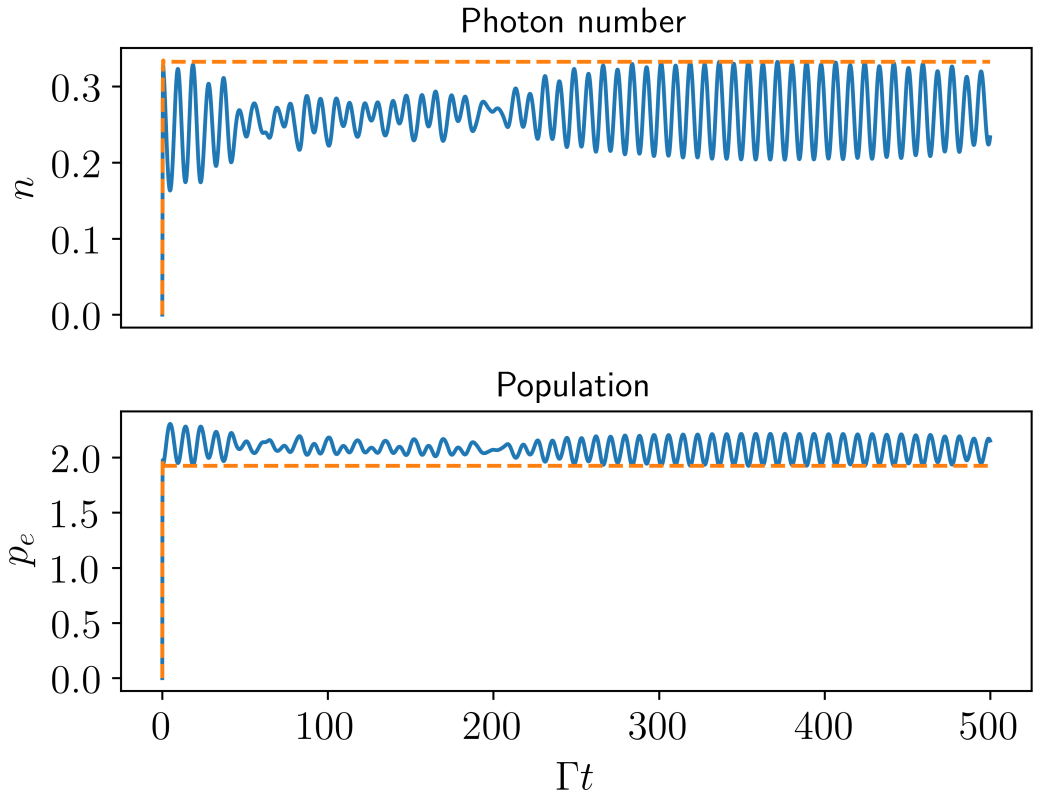

Figure 5.4.: *Time evolution of the photon number (top) and excited state population (bottom).* Both observables almost instanteneously jump to a certain value at the beginning and then only fluctuate. On closer examination you can see that the curves behave in an opposite fashion, if the photon number has a maximum the excited state population has a minimum and vice versa. The dashed orange line corresponds to the time evolution for fixed atoms with their positions at 0, $\lambda_c/2$ and λ_c, from $\Gamma t = 0$ to 500. The parameters are the same as in figure 4.1.

Chapter 6.

Conclusion and Outlook

We included atomic motion as a first step in a semi-classical treatment to the numerical description of a superradiant laser, showing the possibility to cool and trap particles at the favoured positions of maximimal field intensity via a cavity cooling process accompanied by lasing of the system. Specific parameter ranges where cooling is possible have been found and the collective cooling process describing our system was compared to the independent one by demonstrating that for the collective case hotter atoms might cool down faster but do not reach a kinetic energy as low as for independent atoms in the end. The laser properties have been investigated of stable operation parameters with the most relevant result being that cavity length fluctuations affect the spectrum of the laser less compared to conventional lasers. Also, the system operates with a narrow spectrum at less than 0.5 photons inside the resonator. The light field properties do not drastically depend on the motion of the atoms for stable configurations, therefore we conclude that the properties of the laser light could be also calculated for fixed atom positions in a good approximation. The fact that optimal cooling is not achieved with the same set of parameters as the best lasing shows that one has to make a certain compromise.

Due to numerical limitations we focused on a system with only a few atoms inside the cavity arranged in a linear chain. A more realistic model would consider higher particle numbers arranged in a rectangular block instead of a linear chain. For this purpose enlarging the motional degree of freedom from one to three dimensions with magic wavelength optical traps in the two additional dimensions to keep them localized would also be interesting. Including a momentum kick arising from spontaneous emission would definitely be worth examining, since then a more accurate prediction of the final kinetic energy and temperature could be given. Also solving the master equation for a fully quantum mechanical treatment of the system, for a few atoms could bring some additional information. For more particles a mean field approximation would be a possible method to handle the size of the problem. Finally one should think about a more realistic model of the pump mechanism, for example with three/four-level atoms instead of two-level atoms also possibly including collective effects on these additional levels.

Appendices

Appendix A.

Dimensionless Equations for Numerical Simulations

A computer doing a numerical simulation does not know anything about the dimensions of the variables, at least in our case. A straight forward way to not care about the dimension would be to use SI-Units, but calculations in SI-Units can be very unpracticable and inefficient, if the computer has to deal with very small and big numbers at the same time. An alternative way is to write down dimensionless equations with dimensionless variables, optimally all of them being the same order of magnitudes. We show here the dimensionless form of our system describing equations (3.5) - (3.6).

First we need to appoint the reference parameters to gain dimensionless variables, in numerical simulations they will have the value 1. We will modify our equations such that all variables are expressed in terms of these parameters. The dimensionless variables are indicated by a tilde. We choose $k_\mathrm{a} = 1$, $\Gamma = 1$ and $\hbar = 1$, therefore we get the following dimensionless variables:

- spatial coordinate: $r \to \tilde{r} = rk_\mathrm{a}$
- time: $t \to \tilde{t} = t\Gamma$
- frequency and rates: $\omega \to \tilde{\omega} = \omega/\Gamma$ e.g. $\tilde{\kappa} = \kappa/\Gamma$
- momentum: $p \to \tilde{p} = p/(\hbar k_\mathrm{a})$

By replacing $\hbar$ with 1 and inserting the frequencies and rates in terms of Γ we obtain the dimensionless Hamiltonian

$$H = \Delta a^\dagger a + \sum_{i=1}^{N} g(r_i)[a\sigma_i^+ + a^\dagger \sigma_i^-] + \sum_{i \neq j} \Omega_{ij} \sigma_i^+ \sigma_j^- . \tag{A.1}$$

The Liouvillian stays the same and the coupled differential equations are modified the following way. Equation (3.3) is multiplied by k_a/Γ and on the right hand side the factor $\hbar k_\mathrm{a}/(\hbar k_\mathrm{a})$ is inserted

$$\frac{dr_i k_\mathrm{a}}{dt\Gamma} = \frac{p_i}{\hbar k_\mathrm{a}} \frac{\hbar k_\mathrm{a}^2}{m\Gamma}.$$

With the definition of ω_r (2.37) we obtain the dimensionless equation

$$\frac{dr_i}{dt} = 2\omega_\mathrm{r} p_i. \tag{A.2}$$

Equation (3.4) is divided by $\hbar k_\mathrm{a}\Gamma$ to obtain the dimensionless expression

$$\frac{d}{dt}p_i = -\frac{d}{dr_i}\left[g(r_i) \left\langle a\sigma_i^+ + a^\dagger \sigma_i^- \right\rangle + \sum_{i\neq j} \Omega_{ij} \left\langle \sigma_i^+ \sigma_j^- \right\rangle \right]. \tag{A.3}$$

We omit the tilde on all variables, hopefully this is not too confusing. This means the r_i is given in units of $1/k_\mathrm{a}$, t in $1/\Gamma$, p_i in $\hbar k_\mathrm{a}$ and all rates in Γ.

Appendix B.

Program Example

We show a Julia code example, using the quantum optics toolbox QuantumOptics.jl [20], for a stable configuration. For all gained data in this thesis the description of the physical model is always as in this example code. We us Julia 1.0.2 and QuantumOptics.jl 0.6.3.

```
#import needed libraries
using QuantumOptics #simulation
using LsqFit #fit spectrum
using DelimitedFiles #save data

#defining variables and parameters
n_p = 3 #photonen cutoff
N_a = 3 #number of atoms

#all variables and parameters are given in units of the following three
Γ = 1.0 #spontaneous emission rate
k = 1.0 #wavevector of the atom transition and the cavity field
ħ = 1.0 #Planck constant

ω_r = 0.1Γ #recoil frequency
Δ = 5.0Γ #cavity atom detuning Δ = ω_c - ω_a
g = 5.0Γ #coupling constant
κ = 20Γ #20 #cavity loss rate
R = 8.0Γ #pump rate
λ = 2π/k #wavelength
θ = π/2 #angel of the dipole vector

#defining the basis of the Hilbertspace
b_c = FockBasis(n_p) #Fockbasis (cavity field)
b_a = SpinBasis(1//2) #2-level basis (atom)
b_all = tensor([b_a for i=1:N_a]...)⊗b_c #complete joint quantum basis

#defining operators
```

```
a = embed(b_all, N_a + 1, destroy(b_c)) #field annihilation operator
ad = dagger(a) #field creation operator
sm = [[embed(b_all, i, sigmam(b_a)) for i=1:N_a]...] #array of atom σ- operators
sp = dagger.(sm) #array of atom σ+ operators

#for faster computation we precalculate frequently used operator products
smad = [[sm[i]*ad for i=1:N_a]...]
spa = dagger.(smad)
spsm = sp.*sm
ada = ad*a
spsm_ar = [sp[i]*sm[j] for i=1:N_a, j=1:N_a]
spa_plus_smad = spa + smad

#initial state
d_atoms = 0.5 #initial atom spacing
#initial classical position and momentum of the atoms:
u = ComplexF64[[0.0, d_atoms, 2d_atoms]λ...,[1.7, -1.6, 1.5]ħ*k...]
#initial semi-classical state: all spins down and 0 photons + classical variables
ψ = semiclassical.State(tensor([spindown(b_a) for i=1:N_a]...,fockstate(b_c, 0)),u)

#defining mathematical functions
ϵ_pos = 0.01/k #smallest distance for correct values

function Ω_ij(r_i, r_j) #coherent dipole-dipole coupling
    if abs(r_i-r_j) < ϵ_pos #includes Ω_ii = 0
        Ω_ij = 0
    else
        ξ = k*abs(r_i-r_j)
        Ω_ij = Γ*(-3/4)*( (1-(cos(θ))^2)*cos(ξ)/ξ
        -(1-3*(cos(θ))^2)*(sin(ξ)/(ξ^2)+(cos(ξ)/(ξ^3))) )
    end
    return real(Ω_ij)
end

function dΩ_ij(r_i, r_j) #derivative of Ω_ij on r_i (same for r_j)
    if abs(r_i-r_j) < ϵ_pos
        dΩ_ij = 0
    else
        ξ = k*abs(r_i-r_j)
        dΩ_ij = -(Γ*3/4)*(-(1-3*cos(θ)^2)*(-(3*sin(ξ))/((ξ)^2*(r_i-r_j))
        +cos(ξ)/(ξ*(r_i-r_j))-(3*cos(ξ))/((ξ)^3*(r_i-r_j)))
        -((1-cos(θ)^2)*sin(ξ))/(r_i-r_j)-((1-cos(θ)^2)*cos(ξ))/(ξ*(r_i-r_j)))
```

```
    end
    return real(dΩ_ij)
end

function Γ_ij(r_i, r_j) #collective decay rate
    if abs(r_i-r_j) < ϵ_pos
        Γ_ij = Γ
    else
        ξ = k*abs(r_i-r_j)
        Γ_ij = Γ*(3/2)*( (1-(cos(θ))^2)*sin(ξ)/ξ
        +(1-3*(cos(θ))^2)*((cos(ξ)/(ξ^2))-(sin(ξ)/(ξ^3))) )
    end
    return real(Γ_ij)
end

#Hamilton operator
function H_dd(x) #coherent dipole-dipole interaction Hamiltonian
    H_dd_ij = 0*spsm_ar[1,1]
    for i=1:N_a
        for j=1:N_a
            H_dd_ij += Ω_ij(x[i], x[j])*spsm_ar[i,j]
        end
    end
    return H_dd_ij
end
H0 = Δ*ad*a #field and two-level atom Hamiltonian in rotaing frame

#Jump-Operators for Liouvillian
J = [[sm[i] for i=1:N_a]..., [sp[i] for i=1:N_a]..., a]
Jd = dagger.(J)

#calculate rates of the dissipative processes
rates_calc = zeros(Float64, (2N_a+1), (2N_a+1))
#pump rates R (stay constant)
for i=(N_a+1):(2*N_a)
    rates_calc[i,i] = R
end
#cavity decay rate κ (stays constant)
rates_calc[(2*N_a+1),(2*N_a+1)] = κ
#collective decay rate Γ_ij (particle position depending)
function fill_rates(r)
    for i=1:N_a
```

```
        for j=i:N_a
            rates_calc[i,j] = Γ_ij(r[i], r[j])
            rates_calc[j,i] = rates_calc[i,j]
        end
    end
    return rates_calc
end

#function to update the Hammiltonian and jump operators at every timestep
function f_q(t,ψ,u)
    #update H
    H_int = g*sum(cos.(u[1:N_a]*k).*spa_plus_smad)
    H = H0 + H_int + H_dd(u)
    #update rates
    rates = fill_rates(u)
    #J always the same
    return H, J, Jd, rates
end

#function to update classical variables (Ehrenfest-theorem)
function f_cl(t,ψ,u,du)
    #update position
    for i = 1:N_a
        du[i] = 2*ω_r*u[N_a + i]
    end
    #update momentum
    for i = 1:N_a
        du[N_a + i] = 1/k*2*g*sin(u[i]*k)*real(expect(spa[i],ψ))
        -1/k^2*sum(dΩ_ij(u[i],u[j])*(2*real(expect(sp[i]*sm[j],ψ))) for j=1:N_a)
    end
end

#semi-classical time evolution
timestep = 0.1
t_max = 1000
T=[0:timestep:t_max;]/Γ
t,ρt = semiclassical.master_dynamic(T,ψ,f_q,f_cl)

#analyzing data
r = [[Float64[] for i=1:N_a]...] #postions of the particles at every timestep
p = [[Float64[] for i=1:N_a]...] #momenta of the particles
E_kin = [[Float64[] for i=1:N_a]...] #kinetic energies of the particles
```

```
n = Float64[] #number of photons in the cavity
popu = [[Float64[] for i=1:N_a]...] #excited state population of the particles
g2_0 = Float64[] #second order correlation function

for it=1:N_a
    r[it] = [ρt[i].classical[it] for i=1:length(ρt)]
    p[it] = [ρt[i].classical[N_a + it] for i=1:length(ρt)]
    E_kin[it] = [(ρt[i].classical[N_a + it])^2 for i=1:length(ρt)]
    popu[it] = [real(expect(spsm[it],ρt[i])) for i=1:length(ρt)]
end
n = [real(expect(ada,ρt[i])) for i=1:length(ρt)]
g2_0=[real(expect(ad*ad*a*a,ρt[i])/(expect(ada,ρt[i]))^2)
    for i=[2,[2:1:length(ρt);]...]]
E_kin_all = sum(E_kin) #overall kinetic energy

#Method to obtain average kinetic energy
function findlocalmaxima(signal::Vector)
    inds = Int[]
    if length(signal)>1
        if signal[1]>signal[2]
            push!(inds,1)
        end
        for i=2:length(signal)-1
            if signal[i-1]<signal[i]>signal[i+1]
                push!(inds,i)
            end
        end
    end
    inds
end

function findlocalminima(signal::Vector)
    inds = Int[]
    if length(signal)>1
        if signal[1]<signal[2]
            push!(inds,1)
        end
        for i=2:length(signal)-1
            if signal[i-1]>signal[i]<signal[i+1]
                push!(inds,i)
            end
        end
```

```
    end
    inds
end

#calulate indices, values and corresponding times of the extrema
ind_extr = sort([findlocalmaxima(E_kin_all)..., findlocalminima(E_kin_all)...])
t_kin_average = [(t[ind_extr[i]] + t[ind_extr[i+1]])/2 for i=1:length(ind_extr)-1]
E_kin_average = [(E_kin_all[ind_extr[i]]+E_kin_all[ind_extr[i+1]])/2
    for i=1:length(ind_extr)-1]

#calculate semiclassical spectrum - might take some minutes
timestep2 = 0.005
τ = [0:timestep2:20;] #20 → 60 for higher accuracy
αρ0 = semiclassical.State(a*ρt[end].quantum, ρt[end].classical)
t2, ρt2 = semiclassical.master_dynamic(τ,αρ0,f_q,f_cl)
corr = expect(ad, ρt2)
ω, spec = timecorrelations.correlation2spectrum(t2, corr)
spec_norm = spec/maximum(spec)

#lorentz fit
@. lorentz(ω_lor, par) = par[3]*par[2]^2 ./((ω_lor-par[1]).^2 + par[2]^2) + par[4]
#p[1] = offset, p[2] = HWHM, p[3] = amplitude, p[4] = intensity offset
par0 = [0.1,0.1,0.1, 0.0001]
fit = curve_fit(lorentz, ω, spec_norm, par0)
lorentz_fit = lorentz(ω, fit.param)

#save the data
writedlm("time.txt", t, ", ")
writedlm("photon_number.txt", n, ", ")
writedlm("population.txt", popu, ", ")
writedlm("coherence.txt", g2_0, ", ")
writedlm("position_part_1.txt", r[1], ", ")
writedlm("position_part_2.txt", r[2], ", ")
writedlm("position_part_3.txt", r[3], ", ")
writedlm("E_kin_all.txt", E_kin_all, ", ")
writedlm("t_kin_average.txt", t_kin_average, ", ")
writedlm("E_kin_average.txt", E_kin_average, ", ")
writedlm("omega_arr_spec.txt", ω, ", ")
writedlm("spec_norm.txt", spec_norm, ", ")
writedlm("lorentz_fit.txt", lorentz_fit, ", ")
```

Bibliography

[1] Justin G. Bohnet, Zilong Chen, Joshua M Weiner, Dominic Meiser, Murray J. Holland, and James K. Thompson. A steady-state superradiant laser with less than one intracavity photon. *Nature*, 484:78–81, 2012.

[2] D. Meiser, Jun Ye, D. R. Carlson, and M. J. Holland. Prospects for a millihertz-linewidth laser. *Phys. Rev. Lett.*, 102:163601, 2009.

[3] V. Vuletic. An almost lightless laser. *Nature*, 484:43–44, 2012.

[4] F. Haake, M. I. Kolobov, C. Fabre, E. Giacobino, and S. Reynaud. Superradiant laser. *Phys. Rev. Lett.*, 71:995–998, 1993.

[5] R. H. Dicke. Coherence in spontaneous radiation processes. *Phys. Rev.*, 93:99–110, 1954.

[6] M. Gross and S. Haroche. Superradiance: An essay on the theory of collective spontaneous emission. *Physics Reports*, 93(5):301–396, 1982.

[7] T. Maier, S. Krämer, L. Ostermann, and H. Ritsch. A superradiant clock laser on a magic wavelength optical lattice. *Optics express*, 22 11:13269–79, 2014.

[8] T. Salzburger and H. Ritsch. Atomic self-trapping induced by single-atom lasing. *Phys. Rev. Lett.*, 93:063002, 2004.

[9] T. Salzburger and H. Ritsch. Lasing and cooling in a finite-temperature cavity. *Phys. Rev. A*, 74:033806, 2006.

[10] S. Haroche and J.-M. Raimond. *Exploring the Quantum*. Oxford University Press, 2013.

[11] R. R. Puri. *Mathematical methods of quantum optics*. Springer Berlin Heidelberg, 2001.

[12] H.-P Breuer and F. Petruccione. *The Theory of Open Quantum Systems*. Oxford University Press, 2006.

[13] V. Weisskopf and E. Wigner. Berechnung der natürlichen linienbreite auf grund der diracschen lichttheorie. *Zeitschrift für Physik*, 63(1):54–73, 1930.

[14] Z. Ficek and R. Tanaś. Entangled states and collective nonclassical effects in two-atom systems. *Physics Reports*, 372(5):369 – 443, 2002.

[15] L. Ostermann. *Collective Radiation of Coupled Atomic Dipoles and the Precise Measurement of Time*. Dissertation, Institut für Theoretische Physik, Universität Innsbruck, 2016.

[16] A. Galindo and P. Pascual. *Quantum Mechanics I*. Springer-Verlag Berlin Heidelberg, 1990.

[17] H. Ritsch, P. Domokos, F. Brennecke, and T. Esslinger. Cold atoms in cavity-generated dynamical optical potentials. *Rev. Mod. Phys.*, 85:553–601, 2013.

[18] B. Saleh and M. Teich. *Fundamental of Photonics*. John Wiley & Sons, Inc., 1991.

[19] D.F. Walls and G. J. Milburn. *Quantum Optics*. Springer-Verlag Berlin Heidelberg, 2008.

[20] S. Krämer, D. Plankensteiner, L. Ostermann, and H. Ritsch. Quantumoptics. jl: A julia framework for simulating open quantum systems. *Comp. Phys. Comm.*, 227:109–116, 2018.